

Design and Development of Virtual Environments for
Assessment and Treatment of Head Movement and Gaze
Dysfunction in Vestibular Disease

by

Honglu Xu

Submitted in partial fulfillment of the requirements
for the degree of Master of Science

Thesis Advisors:

Michael J. Fu, PhD

Mark F. Walker, MD

Department of Computer and Information Science
CASE WESTERN RESERVE UNIVERSITY

December, 2020

Contents

List of Figures	v
Abbreviations	vi
Abstract	vii
1 Introduction	1
1.1 Thesis Contributions	2
1.2 Thesis Outline	2
2 Background	3
2.1 Vestibulo-ocular reflex	3
2.2 Vestibulo-ocular dysfunction	7
2.3 Vestibulo-ocular assessments	9
2.4 Gaze shifts	13
2.5 Vestibular rehabilitation	14
2.6 Virtual environment for assessment and rehabilitation	15
3 Software development	18
3.1 Dynamic VOR Assessment	18
3.1.1 System Data Flows	18
3.1.2 Component Descriptions	23

3.2 Head Rotation Training Video Games	35
3.2.1 System Data Flows	35
3.2.2 Component Descriptions	36
4 VOR Assessment Experimental Methods	48
4.1 Subjects	48
4.2 Assessment Software Design	48
4.2.1 General Assessment Experiment Paradigm	49
4.2.2 Static Visual Acuity Assessment	50
4.2.3 Dynamic Visual Acuity Assessment	52
4.2.4 Temporal Visual Dynamic Acuity Assessment	54
4.2.5 Temporal Gaze-Shift Visual Acuity Assessment	56
4.2.6 Temporal Assessment With Eye Data	59
5 Results	60
5.1 Static Visual Acuity Assessment	60
5.2 Dynamic Visual Acuity Assessment	62
5.3 Temporal Dynamic Vision Acuity Assessments	64
5.4 Temporal Gaze-shift Acuity	66
5.5 Head-turn trajectory measurement	69
6 Discussion	83
6.1 Key Findings	83
6.2 Conclusion	86
6.3 Limitation and Future Work	86
Bibliography	88

List of Figures

2.1	Inner ear vestibular organs. [1]	4
2.2	Demonstration of the rotation of an object. [2]	5
2.3	Cupula and hair cell. [3]	5
2.4	VOR neural pathway	6
2.5	Model of VOR with cerebellum system	7
2.6	Example of a scleral lens and magnetic frame. Figure A: magnetic frame; Figure B: scleral lens	11
2.7	Examples of the Tumbling E (left), and Landolt-C (right).	13
2.8	An example for Computerized dynamic posturography. [4]	16
3.1	System data flows chart.	18
3.2	Picture of Eye Tracking Glasses.	20
3.3	Functional Illustration of Eye Tracking Glasses.	21
3.4	Xbox Controller button chart.	22
3.5	Picture of The Display Monitor.	23
3.6	Software Design Component Chart.	24
3.7	Example of Animator Controller.	27
3.8	Screen shots of the Dynamic VOR Assessment. Figure A: contents displayed to the staff; Figure B: contents displayed to the participants.	31
3.9	Target System.	32
3.10	Landholdt C Sprites (from size 0 to 9) that used on the experiments.	33

3.11	Diagonal sprite comparison between rotation and custom creation.	34
3.12	Oculus Rift CV1 controller mapping.	36
3.13	Head Rotation Training Video Games Common Components	37
3.14	Menu scene screen capture.	38
3.15	Meteor defense screen capture.	39
3.16	Meteor defense state machine controller.	40
3.17	Ice Fisher screen capture. Figure A: displaying the fish; Figure B: displaying the optotype on the fish,	42
3.18	Ice Fisher state machine controller.	43
3.19	Slicer/Dicer game screen capture.	44
3.20	Food Slice game state machine controller.	45
3.21	Blockbuster game screen capture.	46
3.22	Blockbuster game state machine controller.	47
4.1	System General Flow Diagram.	49
4.2	Static Acuity Flow Diagram.	50
4.3	Dynamic Acuity Flow Diagrams.	53
4.4	Assessment Flows of Dynamic Acuity.	53
4.5	Temporal Dynamic Acuity Flow Diagram.	55
4.6	Temporal Gaze Flow Diagrams.	57
4.7	Temporal Assessment Flows of Gaze Shift.	58
5.1	Static visual acuity results after curve fitting	61
5.2	Comparison between SVA and DVA for all subjects.	62
5.3	Dynamic visual acuity result after curve fitting	63
5.4	Temporal dynamic visual acuity result from a single participant . . .	64
5.5	Temporal dynamic visual acuity results	66
5.6	Temporal gaze-shift visual acuity results	67

5.7	Temporal gaze-shift visual acuity results after curve fitting	68
5.8	Temporal gaze-shift visual acuity results after curve fitting	69
5.9	Orientation data of head, eyes, and gaze during head rotation in temporal dynamic visual acuity	71
5.10	Average orientation data of head, eyes and gaze during head rotation in temporal dynamic visual acuity	74
5.11	Angular velocity data of head, eyes, and gaze during head rotation in temporal dynamic visual acuity	75
5.12	Average angular velocity data of head, eyes and gaze during head rotation in temporal dynamic visual acuity	77
5.13	Combination of the TDVA task from a single subject	78
5.14	Data of head, eyes, and gaze during head rotation in gaze-shift visual acuity tasks	79
5.15	Combination data of gaze-shift task	81

Abbreviations

VOR - Vestibulo-Ocular Reflex

VOD - Vestibulo-Ocular Dysfunction

SCC - Semicircular Canal

UVH - Unilateral Vestibular Hypofunction

BVH - Bilateral Vestibular Hypofunction

NHANES - National Health and Nutrition Examination Survey

HIT - Head Impulse Test

DVA - Dynamic Visual Acuity

SVA - Static Visual Acuity

TDVA - Temporal Dynamic Visual Acuity

TGVA - Temporal Gaze-shift Visual Acuity

VEs - Virtual Environments

PPI - Pixels Per Inch

DOF - Degree Of Freedom

IRB - Institutional Review Boards

best PEST - Best Parameter Estimation by Sequential Testing

AOR - accuracy of the responses

SDAD - Static-Dynamic Acuity Difference

HMD - Head Mounted Display

VR - Virtual Reality

Design and Development of Virtual Environments for Assessment and
Treatment of Head Movement and Gaze Dysfunction in Vestibular
Disease

Abstract

by

Honglu Xu

Vestibular rehabilitation and assessments are currently based on self-reported symptoms, so quantitative methods are needed. This thesis describes the development of a novel vestibular assessment and rehabilitation suite that uses virtual environments. A vestibular assessment interface was designed to assess head-eye movement trajectories as well as vision fixation time during gaze-shifts with simultaneous head rotation. Four virtual reality rehabilitation video games were also developed to train precise head movement. Results from six able-bodied participants examined visual acuity when the head is still and when the head is moving, along with visual fixation time after a gaze shift with 70 degrees of simultaneous head rotation. A negative relationship was observed between visual acuity and head angular velocity. These results provide evidence that this approach is feasible for the assessment of people with vestibular dysfunction and warrants further investigation.

Chapter 1

Introduction

Balance disorders are common among the general population. Vestibular dysfunction is considered the primary cause of balance-disorders. Particularly, vestibulo-ocular dysfunction (VOD), which is primarily caused by the impairment of vestibulo-ocular reflex (VOR), will cause loss of visual acuity and unstable gaze as well as dizziness and nausea. VOR functions to stabilize visual gaze during head rotation movements. Thus, an impaired VOR will negatively affect a person's ability to perform activities of daily living, such as walking or driving.

Although there is a significant focus on assessing and treating VOR impairment, there is a lack of understanding about the gaze behavior of individuals with VOD during gaze shifts. Specifically, it is unclear how long it will take for individuals to recover and stabilize their vision after eye movements with simultaneous head rotation and whether VOR dysfunction can be treated with rehabilitation training and exercises.

Virtual environments have been used for various purposes. Prior studies have used virtual environments for VOR assessments and rehabilitation [5]. However, there is a lack of studies on virtual environment rehabilitation and assessment focusing on gaze shifts, which is an essential function required for activities of daily living.

This thesis's primarily aim is to develop virtual environments and human interfaces to assess visual gaze functions. Furthermore, video games will be developed for treating VOD with rehabilitation training and exercises using stereoscopic immersive head-worn virtual reality displays.

1.1 Thesis Contributions

The VOR assessment methods and rehabilitation virtual environments that are described in this work are novel. First, we developed quantitative assessment tools for evaluating vestibulo-ocular dysfunction temporal characteristics that are new to the field . We also conducted first-of-their kind temporal acuity measurement experiments on six healthy individuals. A relationship between the head-eye trajectory and temporal acuity accuracy was discovered and contributes new information to the literature. Results also revealed new information about re-fixation time for gaze-shift tasks. Second, we also developed four innovative rehabilitation video games that target specific head rotation and eye gaze motions.

1.2 Thesis Outline

The remainder of this thesis is organized as follows. The Background chapter will state relevant topics about vestibulo-ocular dysfunction and existing research. The Methods chapter will describe the experiment and assessment program details. The VOR Assessment Experimental Methods will describe the procedure for the assessment experiments. The Results chapter will state the findings of this study. The Discussion chapter will relate the results to literature, cover clinical implications of the key findings, and suggest future research directions.

Chapter 2

Background

2.1 Vestibulo-ocular reflex

The vestibulo-ocular reflex (VOR) refers to a neural reflex that helps humans and other species maintain gaze stability during head movements. When the head rotates or translates, either passively or actively, this reflex allows the eyes to fixate their gaze in the same direction so that the images projected upon the retina during this movement are still and motion blur is minimized. During the head movement, the VOR either inhibits or excites the appropriate extraocular muscles so that the eyes rotate in the orbits in the direction opposite to the head rotation, holding gaze steady. Thus, this reflex contributes greatly to activities of daily living for people. [6]

The body's primary vestibular sensing organs are located in the paired labyrinths of the left and right inner ears. Each labyrinth consists of the cochlea, the organ of hearing, and five vestibular motion sensors. Figure 2.1 depicts a model of the right labyrinth. This system includes three roughly orthogonal semicircular canals (labeled as "Anterior", "Lateral", and "Posterior" in the figure) that detect head rotations, and two otolith organs (labeled "Utricle" and "Saccule") that sense translational head movements and the head's orientation relative to gravity. Each canal is sensitive to

one axis of the head rotation, which can be decomposed into the roll, pitch, and yaw components, as illustrated in the Figure 2.2. The combination of these three vestibular sensors allows the brain to measure head rotation about any axis.

Figure 2.3 shows the inner view of a single semicircular canal to illustrate how each canal is able to detect head rotation. As head rotation begins, the rotational acceleration causes the labyrinth to turn, while the fluid in the semicircular canal lags behind due to its inertia. As a result, the relative flow of the fluid in the canal causes the cupula (lower-left in Figure 2.3) to be deflected and the stereocilia of the hair cells to bend in a specific direction. This depolarizes the hair cells, causing them to release excitatory neurotransmitters that increase the firing frequency of the associated vestibular nerve.

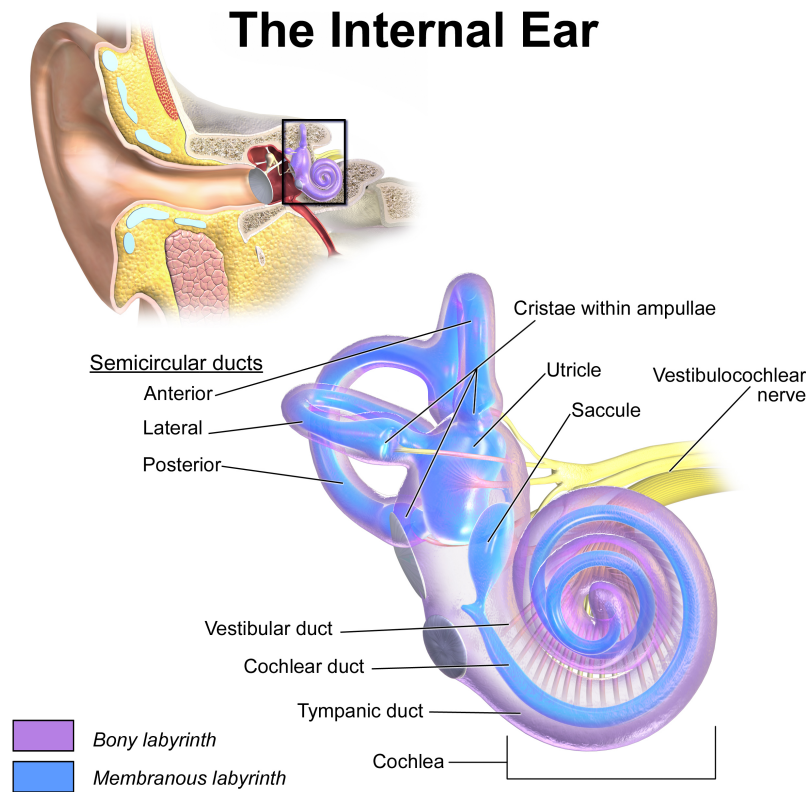


Figure 2.1: Inner ear vestibular organs. [1]

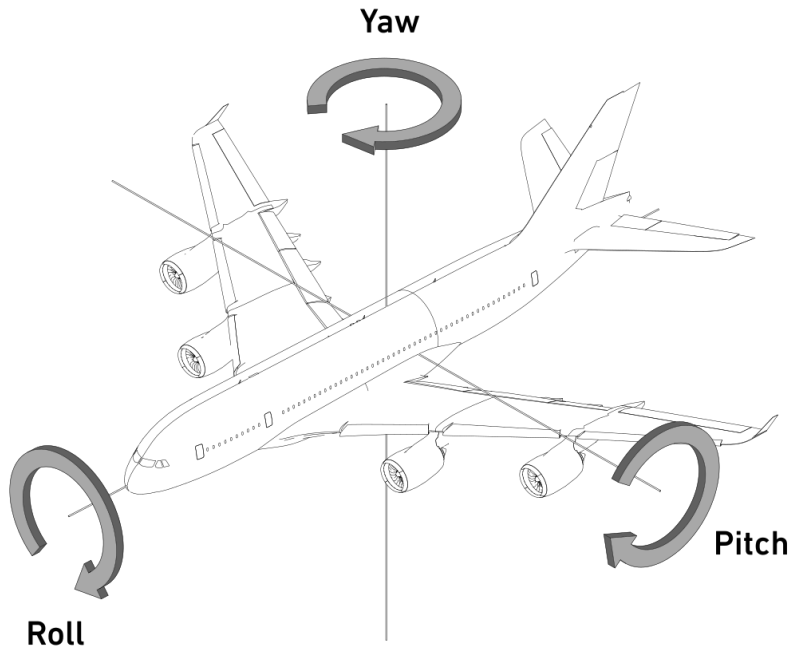


Figure 2.2: Demonstration of the rotation of an object. [2]

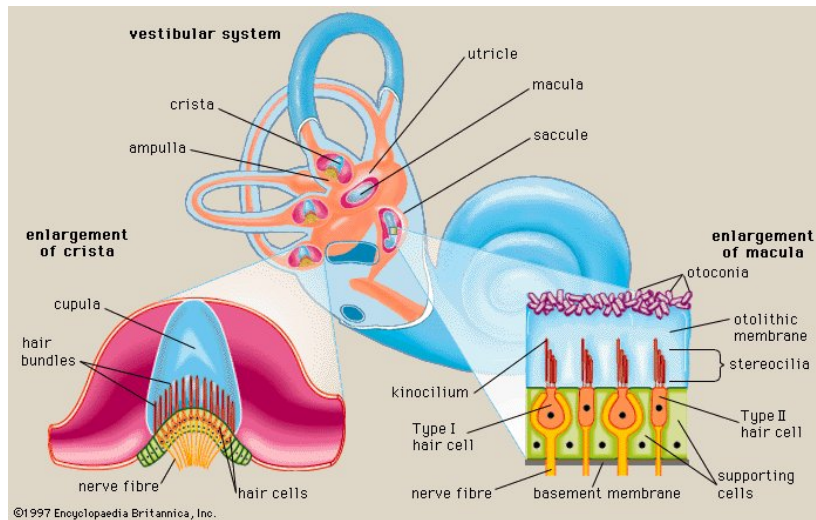


Figure 2.3: Cupula and hair cell. [3]

The monosynaptic excitation from the hair cells will then go through the VOR neural pathway until they reach the extraocular muscles. Figure 2.4 illustrates a model of the neural pathway. As stated before, there are a pair of vestibular sensors, which refers to the left SCC (semicircular canal) and right SCC in the figure. As

the head rotates, in this example, clockwise in the yaw axis, the hair cells in the corresponding semicircular canals will stream out either inhibition or excitation signals depending on the bending direction. Then, as demonstrated in the figure, these signals will go through the pathway and finally reach the corresponding side of the extraocular muscles. The excitation signals (in red) will reach the left side muscles, and the inhibition signals (in blue) will reach the right side muscles. Subsequently, the muscles cause the eyes to make compensatory movements (counter-clockwise in this example) based on the inhibitory or excitatory signal they received. This whole reflex system is continuously working at a high frequency, and thus the response time from the SCC to the extraocular muscles is very short – approximately 12 milliseconds [7].

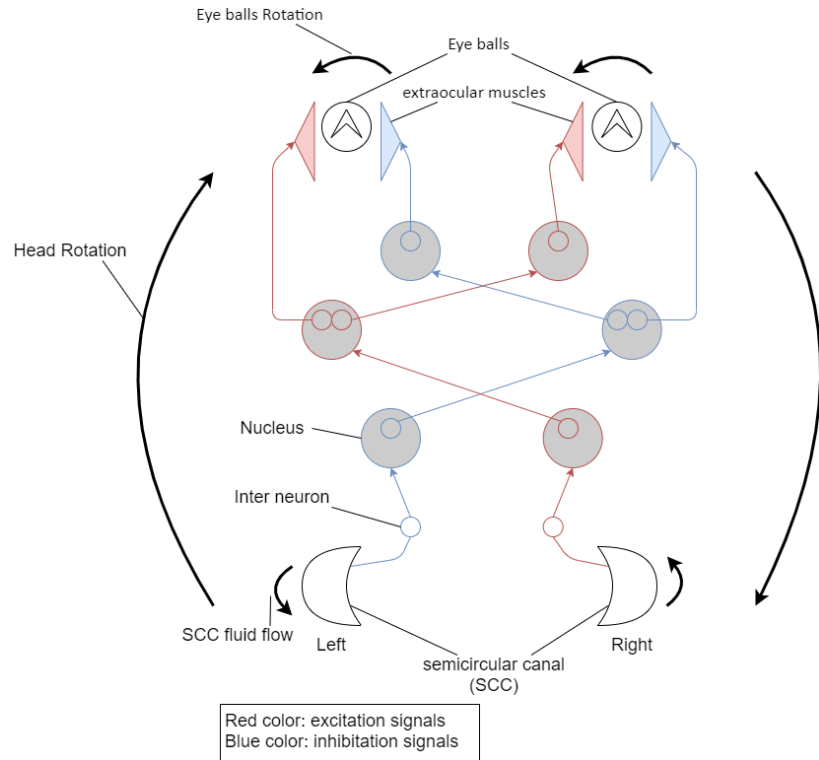


Figure 2.4: VOR neural pathway

In addition, prior studies also suggest that the vestibular system also contributes

to visuospatial function, such as spatial navigation. A group studied some similar vestibular systems on pigeons and ocean fish and concluded that animals might rely on the vestibular system for navigation [8, 9].

Multiple studies have found that the cerebellum, more specifically flocculus, was able to influence the VOR pathway indirectly by altering the weights between the vestibulo sensors and the secondary vestibular neurons [10, 11]. A research group proposed a model of the VOR pathway with the cerebellar system [7], and the main idea is illustrated in Figure 2.5. It is theorized that the cerebellum gathers error signals such as incorrect gaze position and vestibular sensation (represented as the input to the block "Cerebellum") and alters the weighting of the synapse neuron so the eye muscles will receive "better" signals. Research found that this re-weighting process occurs with very short latency. The re-weighting process, referred to as plasticity, has also been shown to occur as a result of vestibular rehabilitation [12].

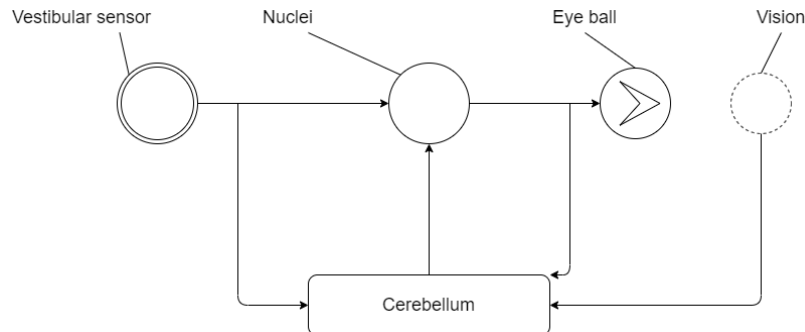


Figure 2.5: Model of VOR with cerebellum system

2.2 Vestibulo-ocular dysfunction

A properly functioning VOR facilitates visual search and stabilizes vision when the head is moving, such as while driving or walking. Thus, impairments of the VOR can cause severe disability and disruption to individuals' lives.

Damage to any of the components along the VOR pathway shown in Figure 2.4

(SCC, pathway neurons, and eye muscles) will cause VOR dysfunction if it is not adequately compensated. Damage to the labyrinth or vestibular nerve on one side of the head is defined as unilateral vestibular hypofunction (UVH). Bilateral vestibular hypofunction (BVH) results from damage to both sides. If vestibular excitation is lower than it should be during head movements, the eyes will not make a sufficient compensatory rotation, which will result in blurred vision caused by oscillopsia, which refers to involuntary eye oscillations that are dis-coordinated with head movement. It will also cause rotational vertigo, an illusion that the head is spinning when it is not.

Other symptoms such as dizziness, imbalance or disequilibrium, and falls may also occur. One-third of vertigo cases presenting to the clinic are due to vestibular dysfunction, and the lifetime prevalence of vestibular vertigo is 7.4% [13, 14]. Research based on the German population found that vestibular vertigo is also more severe than dizziness that is due to other causes and results in more medical consultations [15]. In addition, vertigo can cause another serious problem – falling, which is also very common among elderly individuals. Studies have shown that people with vestibular dysfunction had a 12-fold increase in odds of falling [13, 16, 15, 17]. In community-dwelling older adults with a history of falls, vestibular dysfunction is significantly more prevalent compared to a group of non-fallers [18]. Another study found that treatment for vestibular dysfunction may lead to fewer falls [19]. Falling can result in other serious problems and can be very costly for treatment. The Centers for Disease Control and Prevention concluded that the societal cost for falls totals rose from more than \$19 billion in 2000 to \$55 billion per year in 2019 [20, 21, 22]. Among people with vestibular dysfunction, 44% had changed their habits of driving, and more than half of them stated having difficulties with social activities and daily living [17, 20]. Other studies found that people with vestibular dysfunction may also undergo difficulties with spatial recognition and navigation [23, 24].

VOR dysfunction is prevalent among adults. Data from the 2001-2004 National Health and Nutrition Examination Survey (NHANES) show that 35.4% of U.S. adults over 40 have symptoms consistent with vestibular dysfunction [16]. Contributors to VOR dysfunction include aging, traumatic brain injury or concussion, meningitis or labyrinthitis, use of ototoxic medication, surgical transection, Meniere disease, and diabetes [25, 16, 26, 27]. Aging is one of the most common causes of VOR dysfunction. Studies have shown that people 80 years or older have 8-fold increased odds of having a dysfunctional VOR compared to younger individuals. [28, 15, 29, 30]. One likely cause of aging-related vestibular dysfunction is the degeneration of vestibular hair cells [16, 31, 32, 33, 34, 35]. Models have shown that about 3% of vestibular nucleus loss per decade happens to people after age 40 [36]. Others reported that elderly people might lose 40% of the hair cells in the semicircular canals [37], and structural changes are found on surviving hair cells [38].

2.3 Vestibulo-ocular assessments

Accurate and reliable assessments are needed to diagnose vestibular disorders and predict VOR dysfunction. The head impulse test (HIT), in which the head is turned abruptly either passively or actively, is one of the most widely used measures of semicircular canal function [39]. Key advantages of the HIT include that it can test independently the function of each of the six semicircular canals. Most commonly, the HIT is performed in the yaw plane to test the horizontal canals.

For the passive HIT test, the examiner begins by holding the subject's head still in a natural center position. Then, without warning the subject, the examiner turns the subject's head quickly about 10 to 20 degrees to either the left or right. A healthy VOR causes the subject's eyes to counter-rotate by an equal amount in the orbits, compensating for the head rotation to keep the eyes steady relative to external space.

The active HIT test is performed similarly, but the subject turns their own head. The head rotation thus is more predictable, increasing the accuracy of the compensatory eye movement.

VOR gain, the ratio of eye speed to head speed, is one of the most critical measures of VOR function. For unimpaired VOR, the eyes will counter-rotate with the same speed as head rotation, which results in a VOR gain of 1.0. In most healthy individuals, the passive VOR gain is less than but close to 1.0 and normal gain may depend on age and head angular speed during the tests. [40, 41].

In research settings, eye rotation has been measured by a scleral lens search coil and a magnetic system, as illustrated in Figure 2.6. The scleral coil is worn on the eye like a contact lens. Embedded within it are loops of wire, in which are induced electric currents by the alternating-current magnetic fields. These signals are proportional to the cosine of the orientation of the eye relative to each magnetic field. More recently, advances in high-speed video technology have made it possible to measure eye rotations non-invasively with infrared-sensitive cameras, which avoids the discomfort of coils. Studies have shown that video-based HIT tests have similar results as measurements performed with scleral coils [41].

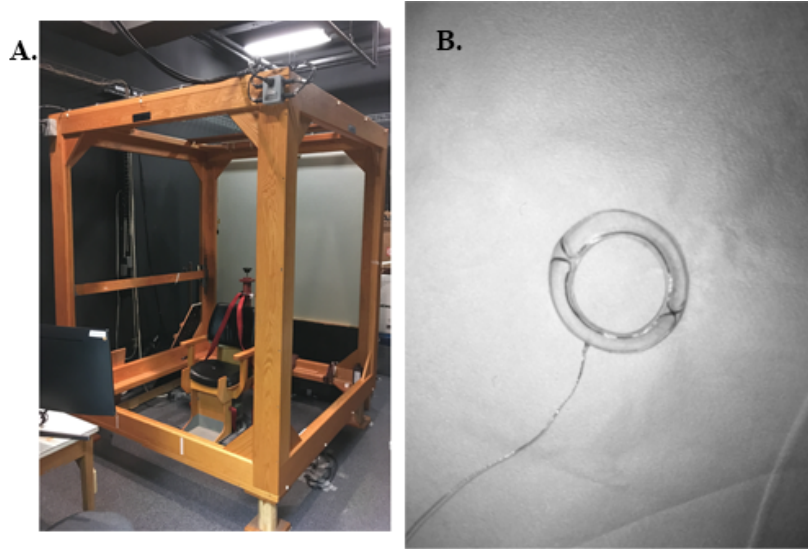


Figure 2.6: Example of a scleral lens and magnetic frame. Figure A: magnetic frame; Figure B: scleral lens

Dynamic visual acuity (DVA) is a complementary method to the HIT for assessing vestibular function. It is a functional test that measures the ability of a person to read symbols or letters, which indicates acuity, while the head is turning. Visual acuity during head motion is compared to static visual acuity (SVA) when the head is still. Both SVA and DVA are measured by the ability to determine the identity or orientation of a letter or symbol as a function of its size. In research, acuity measures are typically based on the orientation of one of two optotypes, the Tumbling-E and the Landolt-C, as illustrated in Figure 2.7. They were both effective for SVA tests [42]. An advantage of the Landolt-C is that it has more orientations and thus a lower false positive rate.

In the active DVA test, the subjects turns the head as would be done for the HIT test. The difference is that optotypes will be presented to the subject while the head is turning. The size of the smallest optotype whose orientation the subject can recognize during head movement is defined as the DVA. An individual with a typical VOR can stabilize vision during the head rotation, such that the DVA for healthy

individuals is very close to the SVA. DVA is an effective tool for detecting vestibular dysfunction [43, 44, 45] and predicting falls [46].

There are two common methods to quantify visual acuity. The Snellen acuity method uses two numbers, such as 20/20. The first number refers to the distance at which the participant must stand to see the same optotype that a typical person can see at the second number's distance. For example, 20/30 means a person needs to stand 20 feet away to see what a typical person could see at 30 feet. Another measure is LogMAR, which is a logarithmic scale based on the smallest visual angle that can be resolved. LogMAR is more suitable for computational acuity measures and can readily represent fractional acuities using the equation

$$L = -\log S, \quad (2.1)$$

where "S" represents the numerical results from the Snellen expression. For example, an optotype representing 20/20 Snellen acuity can be converted to LogMAR by setting S to be 1.0, which results in 0 LogMAR [47].



Figure 2.7: Examples of the Tumbling E (left), and Landolt-C (right).

Although some methods exist for testing the VOR during the head rotation, there is not much focusing on how VOR would affect stabilizing the gaze after the head stopped from a rotation. It is both critical to know whether the vision is stable during head rotation and whether the gaze is on the visual target when the head rotation stops.

2.4 Gaze shifts

Most of the measurements for vestibular function, including HIT and DVA, require the subject to sit still and fix their gaze on a single spot during the tests. During activities of daily living, however, individuals commonly search the environment visually, which shifts the point of fixation from one spot to another in a rapid manner. Such combined

eye-head movements are referred to as gaze shifts.

During a gaze shift, if the angular displacement from one spot to another is small, individuals will usually make only eye movements [48]. This will keep the head still but rotate the eyes to the new gaze target. These rapid eye movements are called saccades. Saccades are not affected by the vestibular system [49]. However, gaze-shift with larger angles would require both head rotation and saccades. Such a gaze shift begins with near simultaneous rotation of the head and eyes. An example of the gaze-shift trajectory and angular velocity that we collected during the experiment is illustrated in Figure 5.14. Since eye saccades are faster than head movements, a compensatory rotation needs to be applied to the eyes after they reach the target, and that is when an accurate VOR is critical. Studies found that individuals with vestibular dysfunction have the tendency to overshoot their gaze or head movement during the gaze shift [50], while others found the opposite results [49]. Thus, the pattern of the head-eye rotation remains unclear, and additional work is needed.

2.5 Vestibular rehabilitation

Treatment of vestibular dysfunction consists of exercises (often referred to as vestibular physical therapy), such as gaze stabilization exercises and static and dynamic balance exercises. [51, 20]

Since error signals can help individuals to re-train the vestibular system, one might assume that people with vestibular dysfunction will spontaneously improve with time, as activities of daily living will also provide error signals. However, it is partially incorrect for multiple reasons. Individuals with vestibular dysfunction tend to lower their social activities, which will lower the amount of time for vestibular exercises. They may also restrict their head movement or blink during head rotations, as they may feel dizziness and nausea. Furthermore, some research suggests that elderly

people tend to need more exercise compared to the younger adults to achieve neuronal change, and some symptoms such as imbalance could last months longer than other symptoms like nystagmus and vertigo [20]. Thus, rehabilitation therapy programs with well-planned schedules could help those individuals greatly.

2.6 Virtual environment for assessment and rehabilitation

Virtual environments, either displayed on monitors or head-mounted displays, have been widely used for various purposes, from entertainment and education to medical and military applications. Multiple vestibular assessment and rehabilitation methods have utilized virtual environments already. Computerized dynamic posturography is one of the rehabilitation methods that have been proven to be effective. An example is illustrated in Figure 2.8, the subjects will be instructed to stand before a monitor, which displays the virtual environment. The subjects wore multiple sensors so they can interact with virtual environment. Feasel, *et al.* combined virtual reality head mounted device with a treadmill system for vestibular rehabilitation and found it is effective in gait asymmetry [5]. Multiple studies also suggested that virtual environment systems could be potentially used for assessments and rehabilitation in the future [20, 52].

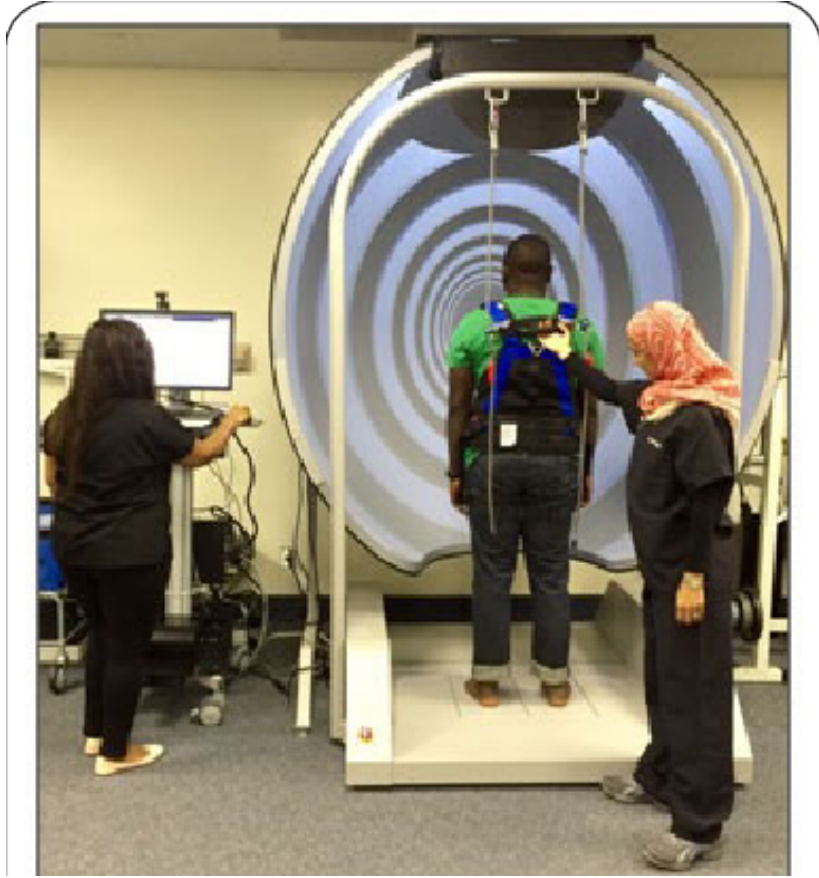


Figure 2.8: An example for Computerized dynamic posturography. [4]

The advantage is that the virtual environment system could provide individually customized and self-administered assessments and rehabilitation. Since virtual environments are software-based, customization is much easier compared to traditional methods such as HIT and DVA tests that are discussed in Section 2.3.

Although traditional assessments are effective in diagnosing vestibular dysfunctions, studies assessing the VOR's influences upon specific activities, such as walking and driving, are still needed [53]. What's more, assessing treatment adherence is one of the most important needs during rehabilitation, and is also much easier to achieve with virtual environment interventions. A research group found that rehabilitation subjects may get better results if the rehabilitation excises is supervised by the clinician [20]. Compared to the control group which was trained without supervision,

the group with supervision scored much better on the dynamic gait index (14% vs. 86%), which is used to measure the degree of in-balance, and other assessments after training. They also stated that the unsupervised program had higher dropout rates. With a virtual environment intervention, subjects' data could be recorded and stored precisely, and assessment and analysis could even be self-administered at home with remote therapist supervision.

Chapter 3

Software development

3.1 Dynamic VOR Assessment

3.1.1 System Data Flows

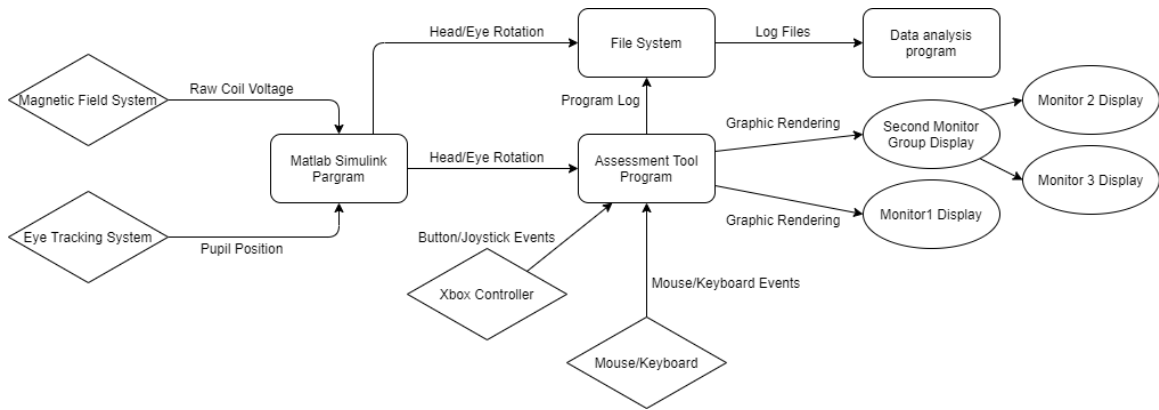


Figure 3.1: System data flows chart.

A series of customized training and assessment virtual environments (VEs) were developed for this study. Since a gaze shift contains two phases: head movement and eye movement, both movements were acquired.

As illustrated in Figure 3.1, there were four motion tracking and input systems used for this purpose: a magnetic field system with coils (CNC Engineering, Inc,

Enfield, CT) detecting head rotations; an eye goggle (I-Scan, South Boston, MA) with high-speed cameras detecting the eye rotations; a controller (Microsoft Corp., Redmond, WA) with joysticks and buttons for visual interface input from the participants, and mouse and keyboard for study staff to adjust experiment parameters and settings. The raw magnetic system input data and raw eye-tracking system input data were streamed to a Matlab real-time Simulink program. Afterwards, the Simulink program calculated and sent out head and eye rotation orientation and angular velocity to the assessment program that was developed with Unity Engine and C# through the UDP stream as interactive input data. Meanwhile, Simulink will also log all the calculated data and save them in files for offline analysis. During the experiment, participants were also required to use the controller's joysticks and buttons to interact with the program, and all those actions will be recorded for offline data analysis. Three monitors were used for displaying contents, two (ANDYCINE, Shenzhen, China) for the participants and one (Dell, Round Rock, TX) for the staff.

Magnetic Field System

A commercial magnetic field system was used to measure head rotation. As discussed in Section 2.1, there are three axes an object can be rotated in space, which are defined as roll, pitch, and yaw (see Figure 2.2).

To track the head rotation in these dimensions, a large frame (Figure 2.6, A) generated three perpendicular AC magnetic fields that surrounded the participant. The magnetic fields were detected by three pairs of two dime-sized perpendicularly-oriented sensing coil wires that are attached to the participant's head (Figure 2.6, B). Since the AC magnetic fields changed their strength constantly, electric currents were generated in these head-worn sensing coil wires, and the intensity was dependent upon the sensing coil orientation among the magnetic fields. Thus, while participants rotate their heads within the magnetic field, the current intensities through the head-

worn sensing coils will change correspondingly. Lastly, the magnetic field system collected this voltage from all coils with a high frequency and streamed it to a Real-time Simulink program, which will be described later in this section.

Eye Tracking System

To detect eye rotation, commercially built pupil tracking glasses with the compatible software were used (illustrated in Figure 3.2).



Figure 3.2: Picture of Eye Tracking Glasses.

These glasses used infrared light to record pupil movement via transparent incident mirrors. The Figure 3.3 illustrated the side view of the eye-tracking goggle. There were two high-speed cameras facing downwards to capture eye images, and thus, to avoid blocking the subject's vision, two transparent mirrors reflect the eye images to the camera.

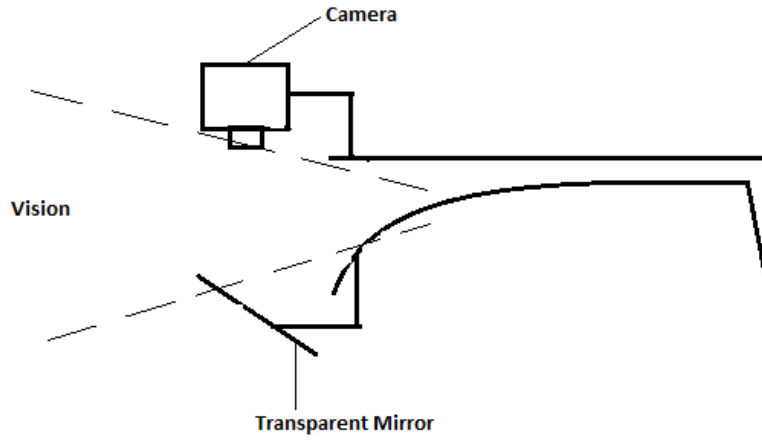


Figure 3.3: Functional Illustration of Eye Tracking Glasses.

After receiving the images, the compatible software and hardware system processed these images and detected the relative pupil positions. Then, the software converted these positions data to four voltage signals, horizontal and vertical positions for both eyes, and scaled those signals to the range of -10 V to 10 V, and streamed out to the Simulink program, which will be described later in this section. As mentioned before, three axes are needed to describe a complete rotation of an object, but it was unnecessary and tedious to detect the roll rotation of the eyes for this thesis's purpose.

Matlab Real-time Simulink Program

A Matlab Simulink programming environment custom developed by previous studies of the lab was used. The Simulink program was deployed on a desktop and used to calibrate and interpret the magnetic system and eye-tracking system data. For head rotation orientation the velocity, the Simulink program received the six coils' voltage streamed from the magnetic field system. Then, it converted the result to a quaternion representing the head orientation angle and streamed the samples out through the UDP. The conversion between quaternion and the Euler angles had been

discussed by Hughes [54]. For eye orientation and angular velocity, the program received four voltage data for each sample, and streamed out the data directly. The Simulink system could stream both head and eye data in 960HZ. The program also log down calibrated orientation and velocity to the file system with the same frequency. It was intended to implement a high-frequency system to gather and log the head and eye rotations.

Controller Input System

A wireless Xbox controller shown in Figure 3.4 provided participants' input to the virtual environment, and each action on the controller was recorded for further data analysis offline. The controller button layout was also illustrated in the figure. The game acquired input from the left joystick (No.3) and the right shoulder button (No. 10). (see Section 4.2.2)

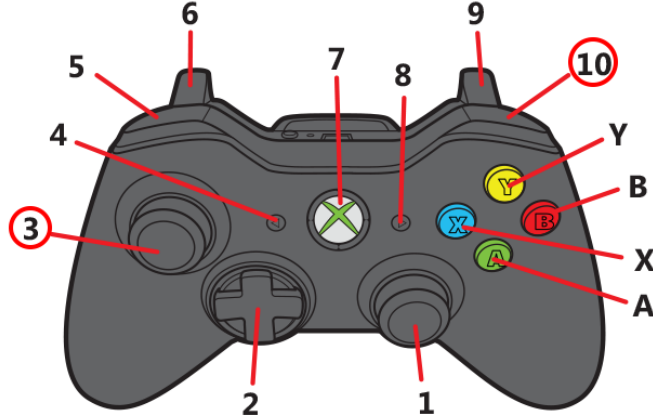


Figure 3.4: Xbox Controller button chart.

Visual Display

The virtual environment was displayed to participants in a otherwise dark room using two 5" IPS monitors as illustrated in Figure 3.5, that were placed around 150 cm away from the participants, and 35 degrees to the left and 35 degrees to the right side from

the participants.



Figure 3.5: Picture of The Display Monitor.

Each monitor had a resolution of 1920x1080, and an aspect ratio of 16:9. The pixel density of these monitors was around 445 pixels per inch (PPI). With these high-density pixel displays, we could test participants with very small optotypes. The smallest (gap of one pixel) optotype that can be displayed by the developed system is equivalent to logMAR -0.88.

3.1.2 Component Descriptions

The VOR functional assessment interface was developed with Unity Engine (Ver. 2018.4.1.f1, Unity Technologies, San Francisco, CA), C#, and .NET 4.0 environment. The overall software architecture is illustrated in Figure 3.6. Each block represents a single component in the program, and the title (first entry for each block) represents the name of the component. The second entry represents the variables that existed in that component, and the third entry included all the functions that were developed in this component. If a line connects two components in the figure, those two

components were able to interact with each other, such as exchange data or sending and receiving events. Since the Unity Engine is a scene-based development engine, the Scene Controller (Figure 3.6 object #1) was used to control the program overall. Initially, the Scene Controller leads participants into an assessment scene where most of the data collection occurred.

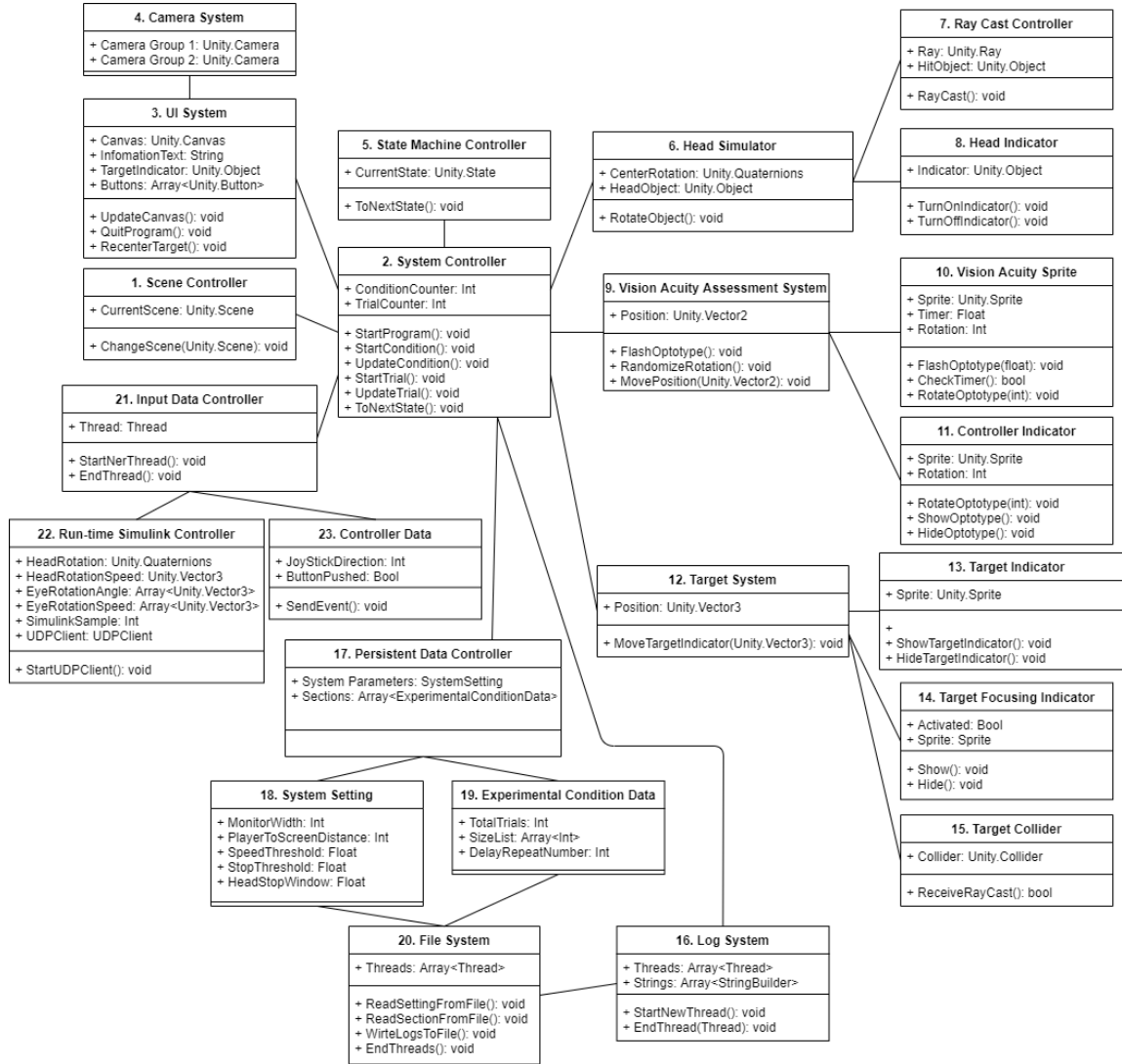


Figure 3.6: Software Design Component Chart.

System Controller

Once in the assessment scene, the System Controller (Figure 3.6 object #2) was the central controller of the whole program. It sent and received events with most of the other components directly or indirectly. It interacted with the UI System (Figure 3.6 object #3) to check whether the button had been clicked and respond by interacting with other components. Also, it interacted with the State Machine Controller (Figure 3.6 object #5) and operated the corresponding function based on the state. With the logical code developed with the variable condition counter and trail counter, the program decided which assessment it should run, and further sent out events to the Vision Acuity System (Figure 3.6 object #9) about the acuity size and display time, as well as to the Target System (Figure 3.6 object #12) about what position it should be moved to. Those data were received from the Persistent Data Controller (Figure 3.6 object #17). When the Xbox controller is used, all the events will be sent into this component from Input Data Controller (Figure 3.6 object #21) and logged with Log System (Figure 3.6 object #16).

The System Controller is also in charge of deciding whether a head turn was valid if the head turn was required in the assessment. To achieve this, three parameters were gathered from System Setting (Figure 3.6 object #18) through the Persistent Data Controller, which were “Speed Threshold,” “Stop Threshold” and “Head Stop Window.” The definition of these parameters will be discussed in Section 3.1.2. When the program was waiting for the participants to turn their heads, it monitored the head speed and head rotation angle from the Run-time Simulink Controller (Figure 3.6 object #22) through the Input Data Controller. Once the absolute horizontal head speed exceeded the Speed Threshold, it would be determined a valid head turn. On the other side, if the horizontal head rotation angle reached a threshold but the speed was not fast enough, this head turn was not valid, and further actions were conducted based on the experimental condition discussed in Section 4.2. After the

valid judgment, the program keeps monitoring the head speed until it was lower than another speed threshold (Stop Threshold). If the speed was lower than the threshold for a certain amount of time (Head Stop Window), it would decide the head was completely stopped. The rationale for this was that most of the participants had subtle head movements just before they completely stopped their heads. Those head movements should be recorded for offline analysis.

State Machine Controller

The State Machine Controller (Figure 3.6 object #5) controlled all state flows of the whole program. The “Current State” variable stored the information of the state index and how this component should interact with the System Controller in the current state, as well as what the next state is. It was driven by the Unity Animator Controller, which an example is illustrated in Figure 3.7, where the states were connected by arrows and conditions judged by the code in the state behavior files attached to the state blocks. All the state flows are similar to the experimental procedures discussed in the Section 4.2. Once a new state was entered, it requested the System Controller for the parameters it needed for this state and send back events to the System Controller about what to do. If a “to next state” signal is received from the System Controller, it would finish the current state and jump to the next state.

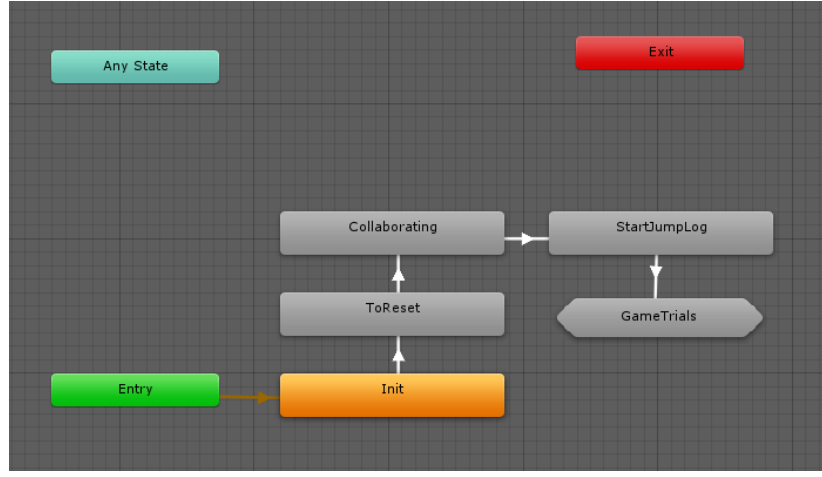


Figure 3.7: Example of Animator Controller.

Persistent Data Controller

The Persistent Data Controller (Figure 3.6 object #17) stored all the variables that need to be used in the complete assessment. Before the System Controller could make any decisions, the data from System Setting (Figure 3.6 object #18) variables and Experimental Condition Data (Figure 3.6 object #19) were needed, which was stored in the Persistent Data Controller and read from the File System (Figure 3.6 object #20). Since there were multiple assessments in a single run, multiple assessments' data were stored in an array, and the index represented the assessments order, which is specified in Section 4.2.

File System

A File System (Figure 3.6 object #20) was implemented for reading and writing data from and into files on hard drives. The System Settings (Figure 3.6 object #18) parameters were stored in a JSON file and de-serialize to a run-time class when the program started, and these data were manually gathered and typed into the JSON file before the program started. It contained: MonitorWidth: Width of the display monitor in center meters; PlayerToScreenDistance: Distance between a participant

and the monitor in center meters; SpeedThreshold: The angular speed to pass the head-turning threshold in degrees per second; StopThreshold: The angular speed to judge whether the head stopped in degrees per second; HeadStopWindow: The time window that judged whether the head stopped completely in seconds.

Additionally, Experimental Condition Data (Figure 3.6 object #19) parameters were stored in a Text file and read by the program line by line. The parameters were: TotalTrials: Total trial number for this assessment; SizeList: A list to contain the optotype size indexes (see Section 3.1.2) information with order; DelayRepeatNumber: Repeat times for each delay period.

The File System handled all the reading and writing events. Before the program ended, it interacted with the Log System (Figure 3.6 object #16) and writes all the log strings to Text files. Since writing the large arrays that contained head motion data to the hard drive caused unwanted halts in the program, multiple threads were created to achieve these tasks. For each task that contained reading or writing files commands, one thread was created and used only for accessing the system file system, and all threads were terminated after the task finished.

Input Data Controller

All input data was controlled by the Input Data Controller (Figure 3.6 object #21) system. To avoid suspending the program while receiving the run-time data with a high frequency (960 HZ), a separate thread was created for Run-time Simulink Controller (Figure 3.6 object #22), which received and unpacked the real-time Simulink data that was received through the UDP port. The Xbox controller input events was also received in the Input Data Controller, but was performed in the program's main thread.

The Run-time Simulink Controller received head and eye orientation and angular velocity from the custom-developed run-time Simulink program deployed on a remote

desktop computer, which collected data from the magnetic field system and eye-tracking glasses, as discussed in Section 3.1.1. The Run-time Simulink Controller was running on a separate thread created by Input Data Controller and updated all variables in a high frequency by receiving data from a UDP client. Once the thread started, it created the UDP client and kept it running through the entire experiment. The variables were: HeadRotation: head rotation in quaternion; HeadRotationSpeed: a Unity built-in Vector3 variable which stored the three axes head rotation speed in degrees per second; EyeRotationAngle: two axes rotations in degrees for both eyes (pitch and yaw); EyeRotationSpeed: 2 axes rotation speeds in degrees per second for both eyes (pitch and yaw); Simulink samples: timestamps generated by Simulink program for synchronizing the time of all the log data; UDP client: a port specified UDP client to receive UDP transmission.

The Controller Data (Figure 3.6 object #23) determined whether the Xbox controller’s joystick was being pushed, and if so, which direction it was being pushed. It also determined whether the Xbox controller’s shoulder button was pressed. Both events were then sent to the System Controller through the Input Data Controller.

UI System

A UI System (Figure 3.6 object #3) was developed that provides two different visual interfaces, one for the participant and one for research staff, along with the System Controller and the Camera System (illustrated in Figure 3.6 object #4). To accomplish this, two Unity Camera groups, which inherited the built-in Unity Engine rendering system, were used in the assessment scene. The first Camera group captured all objects needed to display to the participants and rendered it properly to the dual monitors (Figure 3.8, B). The second Camera group captured mostly the same objects, but instead of rendering to the dual monitors, it rendered to a laptop so that research staff can monitor all the participants’ actions in real-time (Figure 3.8,

A). Different visual interfaces were needed between participants and the staff because some visual objects should be hidden from the participants during the experiment, such as Head Indicator (see Section 3.1.2), but staff should be able to monitor these objects to ensure proper protocol adherence. There was also text information displayed on the staff visual interface that the participants could not see. The text displayed most of the current state information. It contained head rotation angle (see Section 3.1.2), current program state, Target Indicator position (see Section 3.1.2), current experiment condition, current acuity size (see Section 3.1.2), and current acuity delay time. This information helped the staff to monitor participants' performance in real-time and adjust parameters if needed, while not disturbing the participants during the experiment. There were also buttons on the staff's visual interface so that the staff can execute some actions using a computer mouse from the laptop. The "Re-center" button usually was used at the beginning of the experiment to set the Natural Head Position for the program (see Section 4.2.3). The participants were told to focus on the center of the monitor, and by pressing the "Re-center" button, the program recorded this position and calculate all other rotations relative to this Natural Head Position (see Section 3.1.2). The "Quit" button was used to terminate the program. Although all the System Setting and the Experimental Condition data was pre-defined in JSON files by default, it was also possible to change the parameters during the experiment by using the input boxes, drop-down menus, and buttons implemented in this UI System, in case some mistake inputs were done to the files. Also, since there were too many UI components implemented and it was unclear to show all the UI components at the same time, a button called "next page" could iterate all the pages to show the certain UI components, and other UI components that did not belong to that page would be deactivated.

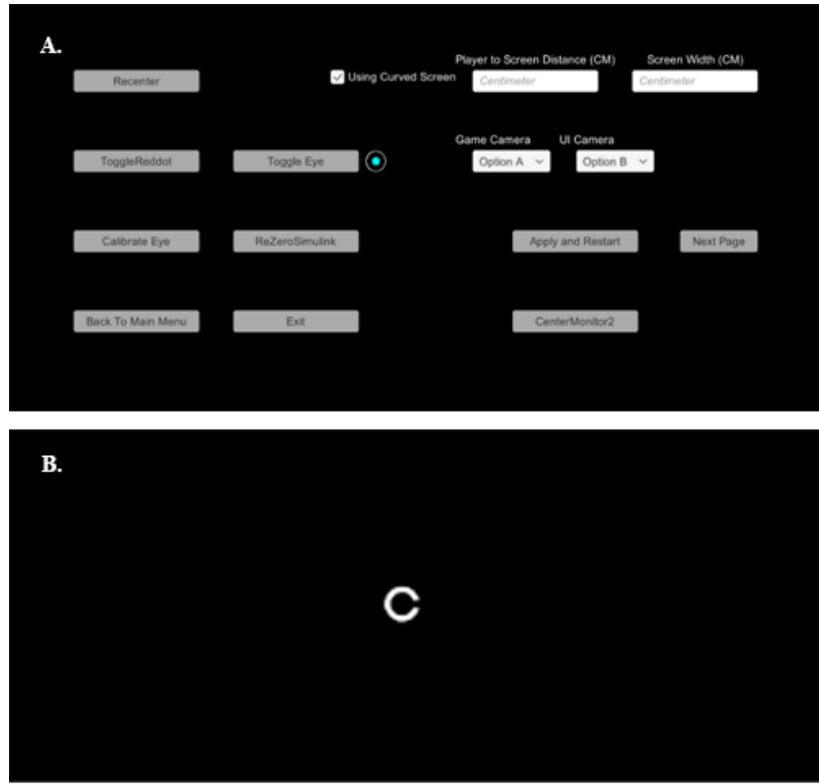


Figure 3.8: Screen shots of the Dynamic VOR Assessment. Figure A: contents displayed to the staff; Figure B: contents displayed to the participants.

Target System

The Target System (Figure 3.6 object #12) generated the main interactive object that participants responded to and provided visual feedback to participants during the assessments. The Target System consists of three parts: Target Indicator (Figure 3.6 object #13), Target Focusing Indicator (Figure 3.6 object #14), and Target Collider (Figure 3.6 object #15), as illustrated in Figure 3.9.

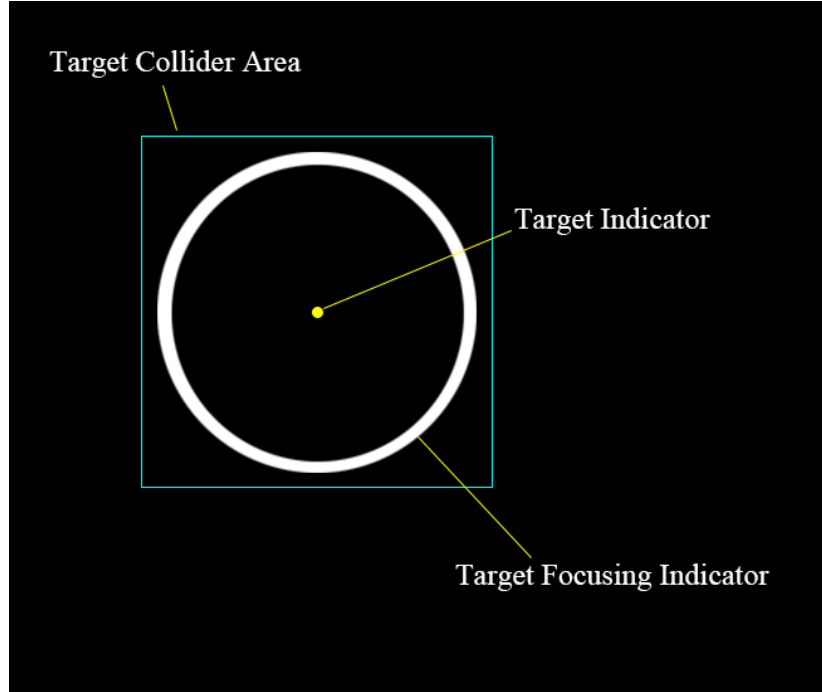


Figure 3.9: Target System.

The Target Indicator was a sphere displayed on the monitor that was used to represent visual targets that the participants were instructed to fixate their gaze upon (see Section 4.2). It also changed color to give signals to the participants when needed. The Target Focusing Indicator, displayed as a 9 cm white circle, visualized and informed the participants they were facing the target. The Target Collider was a Unity Engine built-in Collider component. It detected whether participants achieved the expected head rotation angle for each experiment trial (see Section 4.2). This functionality was implemented using a ray that was cast from a head model (detailed later in this section), which was detected by the Target Collider (see Section 3.1.2).

One challenge of this display system is that the program may not automatically adjust the size and the position of the displayed content, since everything captured by the Unity Camera components (see earlier this section) were rendered to the monitor. To achieve one to one ratio for both content sizes and positions displayed on the dual monitors, we measured and calculated the monitors' field of view and applied it to

the Unity Camera components, so the contents would display the expected contents we needed. The calculation showed in Equation (3.1). The variable “h” represented the physical heights of the monitor, the “D” represented the distance between the monitor and the player, and “F” was the field of view. The idea was to use the height of the monitor and the distance to calculate the view angle of the monitor, and further we would apply this angle to the Unity Camera settings.

$$F = 2 \times \arctan \frac{\frac{1}{2} \times h}{D} \quad (3.1)$$

Vision Acuity Assessment System

The Vision Acuity Assessment System (Figure 3.6 object #9) was another component that produced images for the participants to resolve visually so that their visual acuity could be estimated. As discussed in Section 2.3, there were different types of acuity optotypes, and different sizes were used to measure the visual acuity accurately. The Vision Acuity Sprite (Figure 3.6 object #10) consisted of 2D sprites that were rendered in a pixel-perfect manner calibrated to match the “Landholdt C” visual acuity test symbols, referred to as optotypes that were illustrated in Figure 3.10.



Figure 3.10: Landholdt C Sprites (from size 0 to 9) that used on the experiments.

The main purpose of using this system was to test participants’ static and dynamic

visual acuities. There were 10 optotype sizes, referred to as size index from 0 to 9, and representing visual acuities of logMAR of -0.182, -0.036, 0.072, 0.232, 0.294, 0.397, 0.516, 0.610, 0.709, and 0.808. The smallest optotype used in the experiments was 25 by 25 pixels, which was defined as size index 0. The next larger optotype was around 0.1 logMAR larger. Since the optotypes' sizes were restricted by the limitation that pixel numbers have to be integers, it is not possible to have optotypes differing by 0.1 logMAR increments. However, we could find the optotypes that were closest to this increment. Also, since each optotype size needed to be randomly presented in 8 orientations based on the location of the gap in the circle: 0, 45, 90, 135, 180, 225, 270, and 315 degrees (see Section 4.2), two separate image sets were drawn for each size, one for rotations of 90 degrees and another for rotations of 45 degrees. This was done to reduce distortion caused by rotating the image used for 90-degree orientations by 45 degrees.

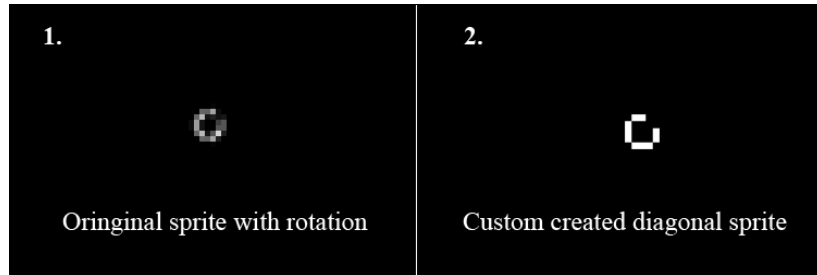


Figure 3.11: Diagonal sprite comparison between rotation and custom creation.

As shown in Figure 3.11, the first sprite, which is generated only by rotating 90-degree orientation sprites, contains pixels other than black and white. This affected the participants' judgment since the gap width was not the same as the orthogonally oriented sprites. In contrast, the custom created sprite on the right side of this figure could keep the gap width constant.

Also, as discussed in Section 4.2.2, to avoid input error, the joystick direction was displayed in the form of a large optotype that participants then need to confirm by

pressing a button on the Xbox controller. The Controller Indicator (Figure 3.6 object #11) was a size index of eight (logMAR 0.709) optotype with a different color (green) that is displayed while participants were pushing the Xbox controller’s joystick.

Head Simulator

The Head Simulator component (Figure 3.6 object #6) is a Unity Object that continuously mimicked the head rotation during the experiment. As explained earlier in this section, the head rotation (Unity Quaternion) was streamed from the Simulink in a high frequency. This object also contains a Ray Cast Controller component (Figure 3.6 object #7), which continuously emitted a Unity Ray toward the forward direction of the head. The Unity Ray could collide with the Unity Collider (see earlier this section) and send event signals to the system, which was handled by the System Controller component.

3.2 Head Rotation Training Video Games

We also utilized a head mounted display VR headset’s immersive feature and implemented multiple games to train participants’ head rotation movements.

3.2.1 System Data Flows

Head mounted VR headset

We used the commercial headset *Oculus Rift CV1* (Facebook, Menlo Park, CA), but the program could be compatible with multiple other devices. (e.g., *Oculus Rift s*, *Valve Index*, etc.) The headset is tracking six degrees of freedom (DOF), which means it could track both rotation and translation for the headset and both hand controllers. The headset was displaying 1080 times 1200 pixels per eye resolution and the screen refresh rate was 90 HZ. There were four buttons on a single controller, see

Figure 3.12, and in the game, we primarily used the Trigger Button. The program listened to the tracking data and button events constantly and respond through the screens. In the meantime, all the actions and data was saved into log files for future analysis. The details will be explained later in this thesis.

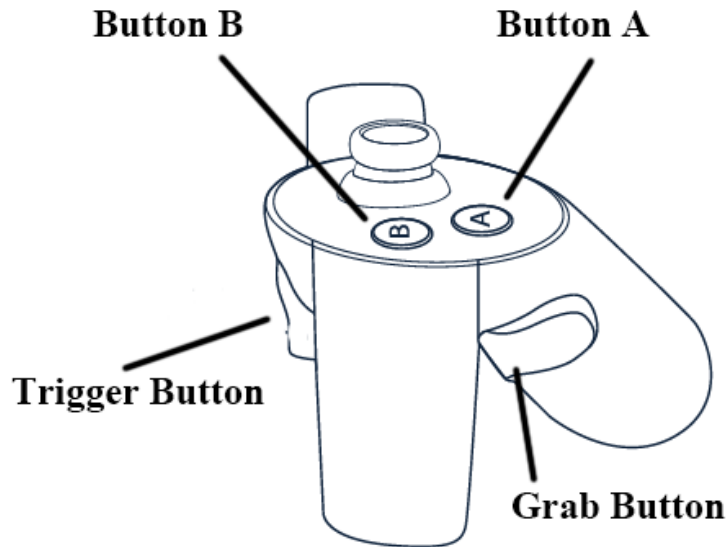


Figure 3.12: Oculus Rift CV1 controller mapping.

3.2.2 Component Descriptions

Common Components

There were four games implemented. Each game has its unique components and motor training goals, but they all contain a set of Common Components. The components were listed in Figure 3.13.

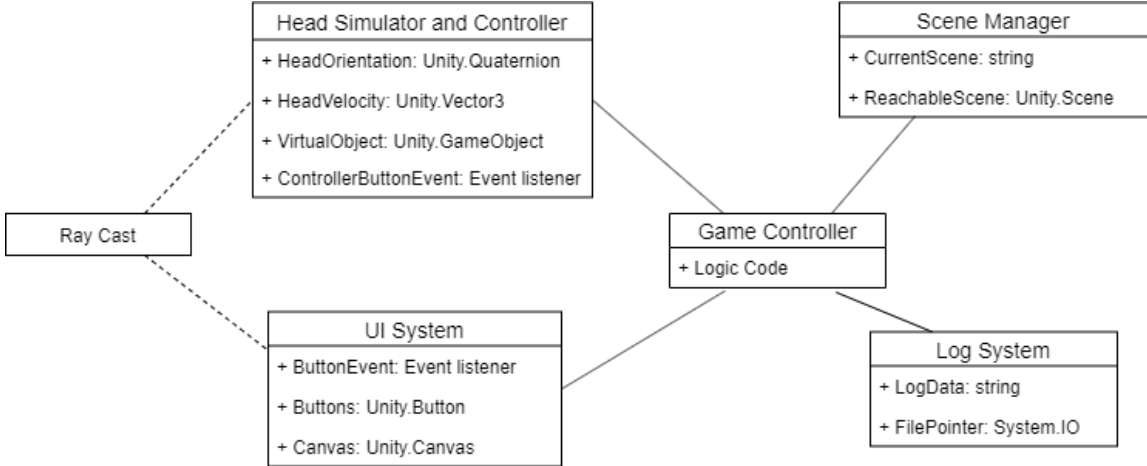


Figure 3.13: Head Rotation Training Video Games Common Components

Head Simulator and Controller: The head simulator component mimicked the head rotation and translation. It contains a Ray Cast component that continuously emitted rays to the forward direction of the head. The details of the Ray Cast component is explained in the Section 3.1.2. The controller's button was mentioned earlier in this section, and this component received and process all the button events.

UI System: The UI System contains UI buttons so the participants could interact with the program. In VR, the system received the Ray Cast components in Head Simulator so the participants could use their head as a cursor.

Scene Manager: The Scene Manager component managed the scene transfer tasks. Each game has its own Unity Scene, so the Scene Manager could lead the participant to the correct Unity Scene based on the game the participants chose to play.

Game Controller: The Game Controller handled and process most of the program logic. It also stored most of the run-time variables. In most cases, it interacted with the State Machine Controller, which will be discussed later.

Log System: The log system took the responsibility to store the head-rotation, button events, acuity (if applicable), and score. At the end of the game, the program accessed the file system and wrote all data to strings in files.

Menu Scene

The Menu Scene was the first scene that showed to the participants when the program first started. It was also presented when participants finished one of the games and exited that game. The primary function of this scene is to help participants navigate through the program. This scene only contains the Common Components that discussed earlier.

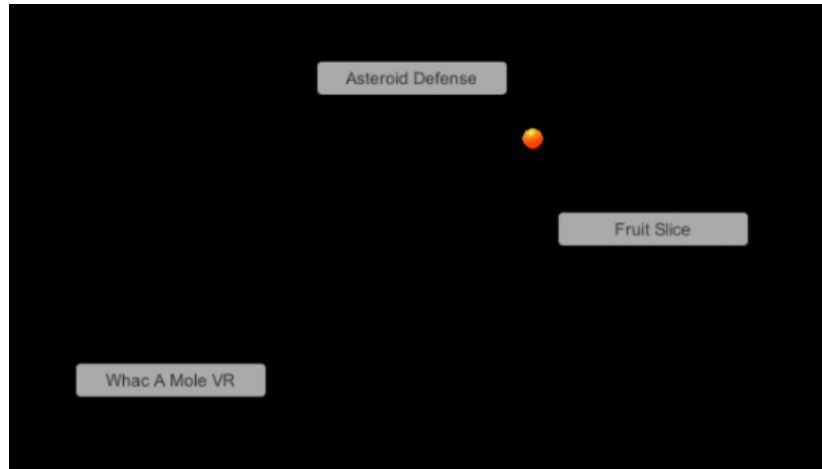


Figure 3.14: Menu scene screen capture.

As shown in Figure 3.14, this scene contains three buttons. The participants could use their head as the cursor and use the Trigger Button on the controller to choose which game to play. Then, the Scene Manager transferred the current scene to a new scene to run the game.

Game: Meteor Defense

The premise of this game is to defend the cities from falling meteors, illustrated in Figure 3.15. The participants need to switch their head rotation between aiming the reload panel and aiming Meteors' trials as each reload panel hit only gave the participant one chance. The game aimed to let the participant practice these fast and accurate large angle multi-point gaze-shifts, which triggered repeated activation of the VOR.

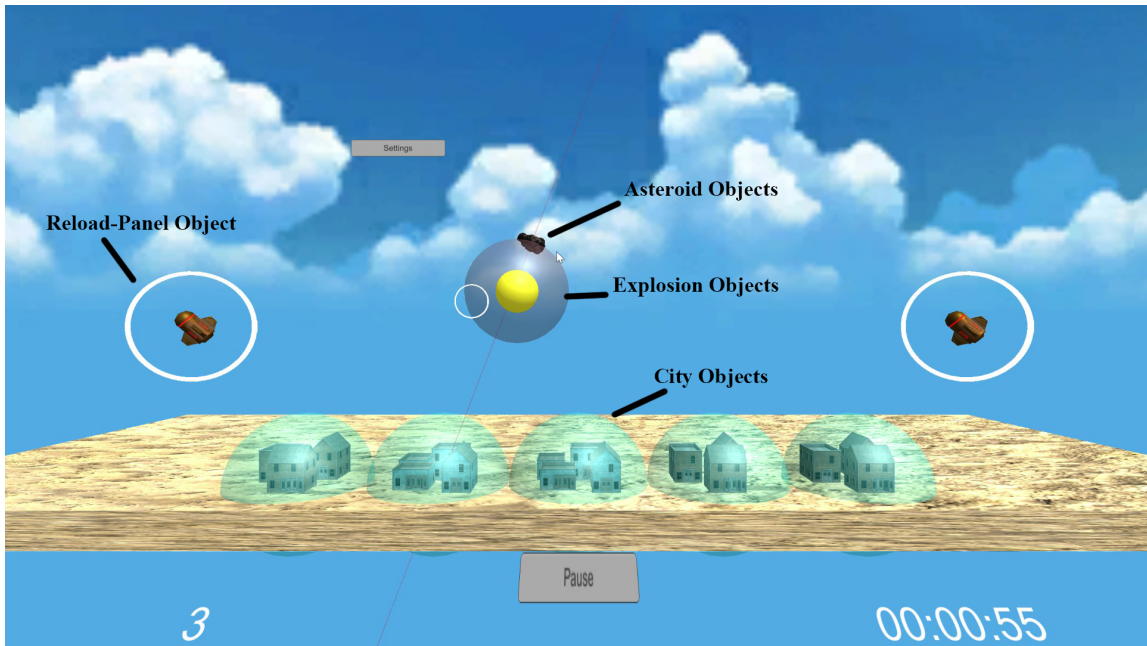


Figure 3.15: Meteor defense screen capture.

Meteor Game Objects System: The Meteor Game Objects System was the primary system to present the game and was controlled directly by the Game Controller. It contains four sub-systems: Meteor Objects, City Objects, Explosion Objects, Reload-panel Objects.

The Meteor Objects were instantiated by the Game Controller and move toward the City Objects. It either was destroyed by colliding with the City Objects or with the Explosion Objects.

The City Objects were instantiated at the start of each level. Each of them contains a variable “health,” which would decrease when the Meteor Objects hit the City Objects. When the “health” went to zero, the City Object would be destroyed.

The Explosion Object was instantiated when the Trigger Button was pressed (if already reloaded). The Explosion position was controlled by the Ray Cast from the Head Simulator that discussed earlier in this section. Thus, the participants were able to use their head as the cursor to control the Explosion Object’s position.

The Reload-panel Objects were fixed on the side of the scene. Participants need to use their head to point to the panel, then press the Trigger Button to activate the reload action. Each reload action allowed the participants to spawn one Explosion Object. That is why participants need to switch between the reload panel and the Meteors’ trials quickly to play the game.

State Machine Controller: The State Machine Controller contains the states for this game. A snapshot was illustrated in Figure 3.16.

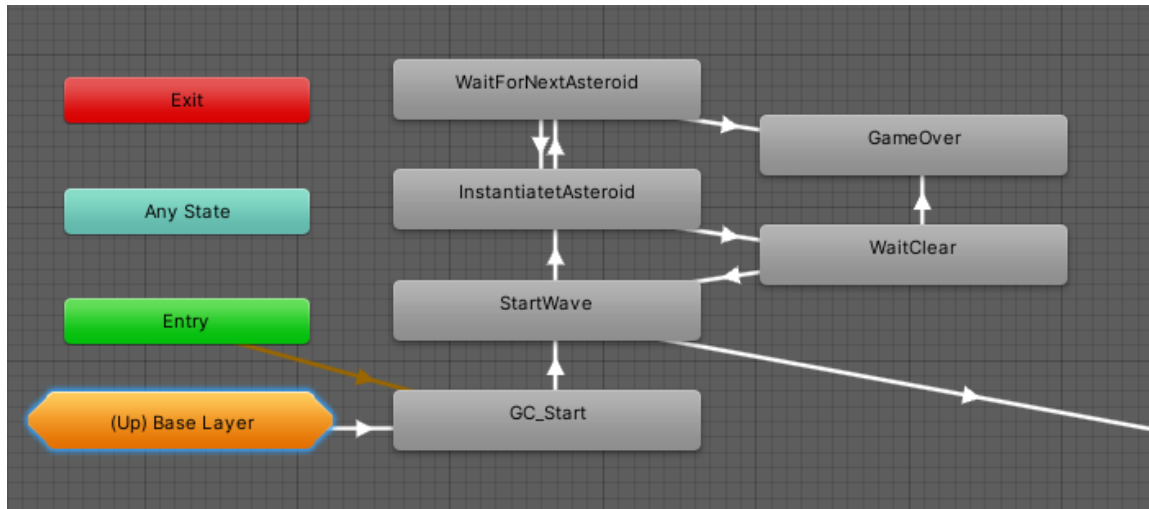


Figure 3.16: Meteor defense state machine controller.

GC Start: start the game. Start Wave: start a new level. Instantiate Asteroid: spawn a new Meteor. Wait For Next Asteroid: wait for the previous Meteor to be

destroyed. Wait Clear: wait for the whole level to be cleared. Game Over: game finished.

Game: Ice Fisher

This game is based on the classic game Whack-a-Mole, but we changed the scenario to a fish catching game. The participants need to use their head to aim at the fish when they jump up from the lake and resolve the optotype that appears on the fish correctly to catch the fish. A screenshot was illustrated in Figure 3.17. This game also requires participants to practice multi-points gaze-shift. However, compared to the Meteor Defense, this game focuses on the challenge of resolving optotypes rather than head rotation accuracy.

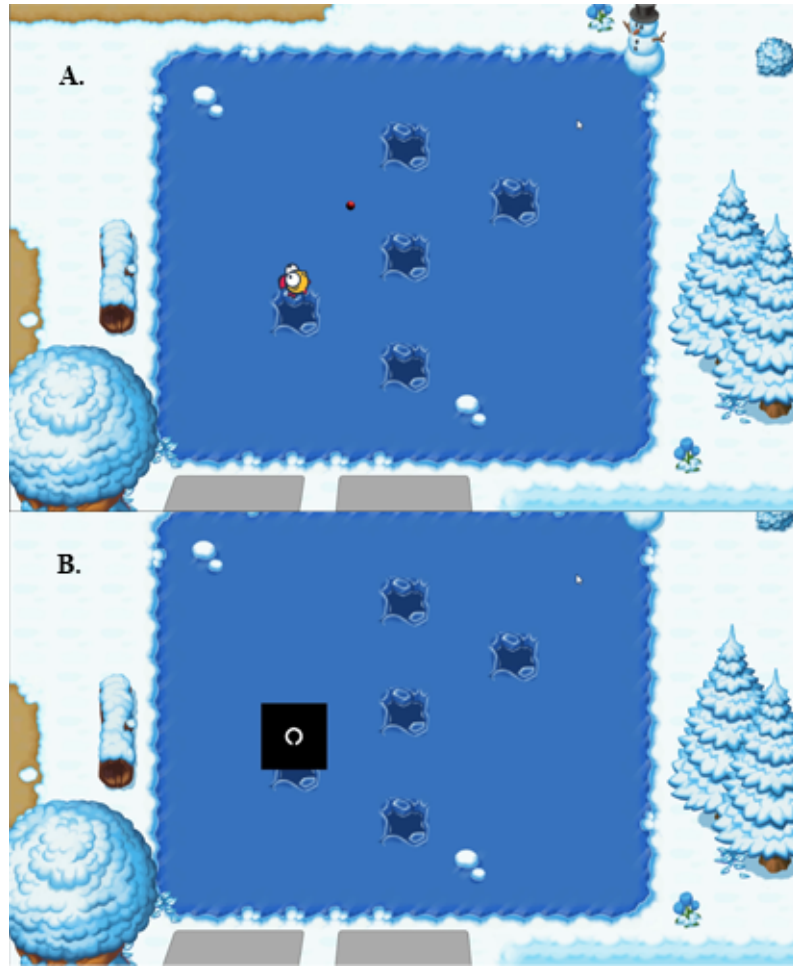


Figure 3.17: Ice Fisher screen capture. Figure A: displaying the fish; Figure B: displaying the optotype on the fish,

Ice Fisher Game Objects System: The Game Objects System was the primary system to present the game. There were three sub-systems in this system: Hole Objects, Fish Objects, and Optotype Objects.

The Hole Objects were instantiated at the start of each level. It represented the potential position that the Fish Objects would spawn.

The Fish Objects will be frequently instantiated by the Game Controller, and the position was randomly chosen from all the Hole Objects that already existed.

When participants used their head to aim at the fishes, an optotype (see Sec-

tion 3.1.2) popped up for 80 ms, and participants would successfully catch the fish if they resolve the optotype correctly.

State Machine Controller: The State Machine Controller contains the states for this game. A snapshot was illustrated in Figure 3.18.

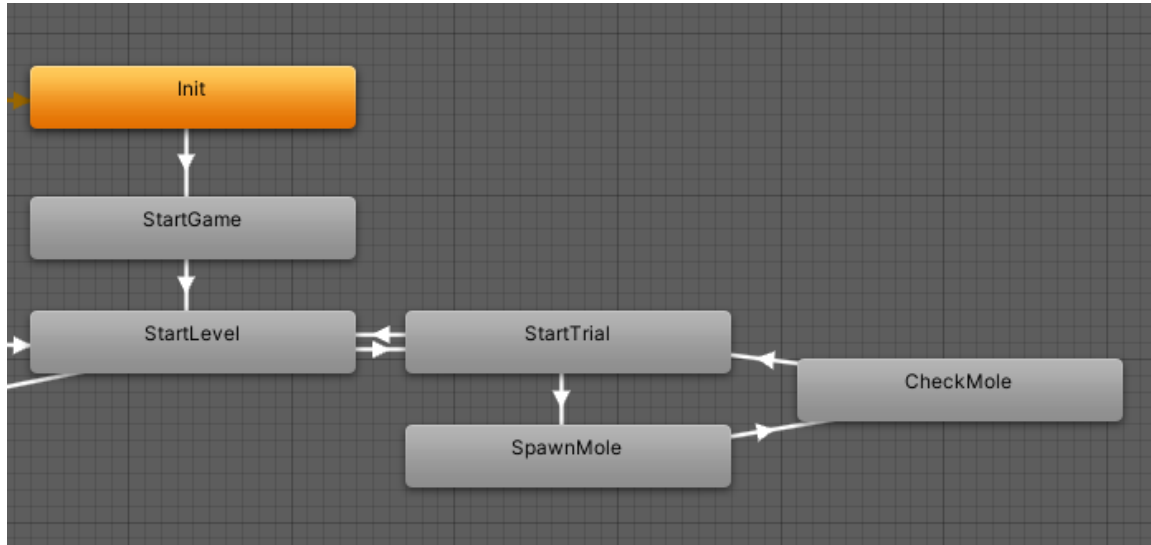


Figure 3.18: Ice Fisher state machine controller.

Start Game: start the game. Start Level: start the level. Start Trial: start a single trial. Spawn Mole: spawn a “mole,” here we spawn a fish. Check Mole: check if the participant successfully whacked the mole (caught the fish).

Game: Slicer/Dicer

The scenario of the game is to allow the participants to slice the food with their head rotation. It requires participants to practice precise control of head turn trajectory and velocity while conducting a natural head rotation and gaze-shift. A screenshot was illustrated in Figure 3.19. The participants will be instructed to rotate their head from one point to another to finish a cut trial. The cutting trajectory will then be recorded and compared to the ideal trajectory, and any difference will deduct the

bonus score, which will be calculated later. After finishing all the cutting trials, the program will compare the shape of each piece to the ideal shape and also deduct the bonus score for differences. The total bonus score then will be calculated to the stars and give feedback to the participants about how well they did. The stars could also be used to unlock the levels with higher difficulties as participants may be ready to get more difficulty training if they did well in the lower difficulty training.

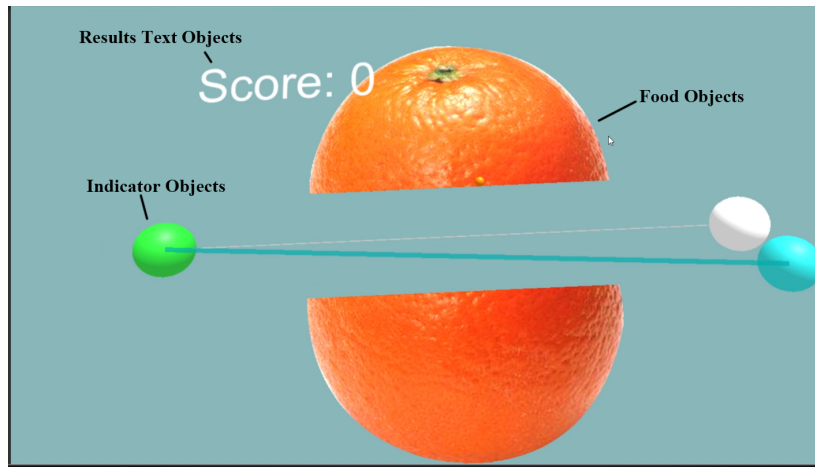


Figure 3.19: Slicer/Dicer game screen capture.

Slicer/Dicer Game Objects System: The Game Objects System was the primary system to present the game. There were four sub-systems in this system, which were: Food Objects, Indicator Objects, Results Text Objects, and Menu Panel Objects.

The Food Objects were instantiated at the start of each level. It visually provides a scenario of what the participants were doing. The Food Objects separated into multiple pieces after the slice action.

The Indicator Objects informed the participants where to aim their head and which direction to slice the food. It was also instantiated at the start of each level.

Results Text Objects were texts that could inform the participants of how well they have done for that level. It gave accurate feedback and help the participants to

improve.

The Menu Panel Objects was presented at the start of the game. Participants could use these panels to choose which level to play.

State Machine Controller: The State Machine Controller contains the states for this game. A snapshot was illustrated in Figure 3.20.

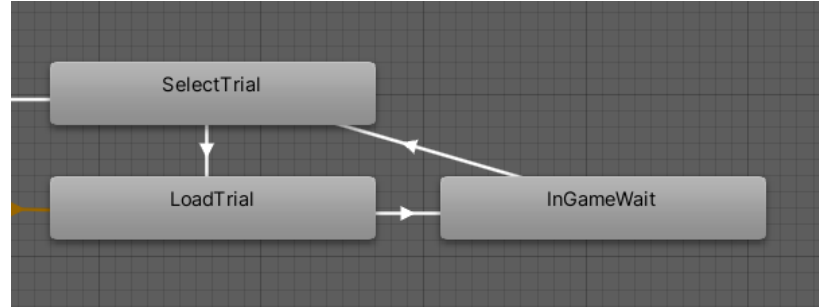


Figure 3.20: Food Slice game state machine controller.

Select Trial: let the participant select which level to play. Load Trial: load information for this level. In Game Wait: wait for this level to finish.

Game: Blockbuster

The Blockbuster originated from a classic game “Breakout.” The participants need to use the head rotation to control a panel to catch a ball, so the ball bounced back and hit/destroy the blocks in the scene. A screenshot was illustrated in Figure 3.21. This game requires participants to practice functional integration of head and eye coordination, point-to-point gaze-shift as well as real-time target tracing gaze movements.

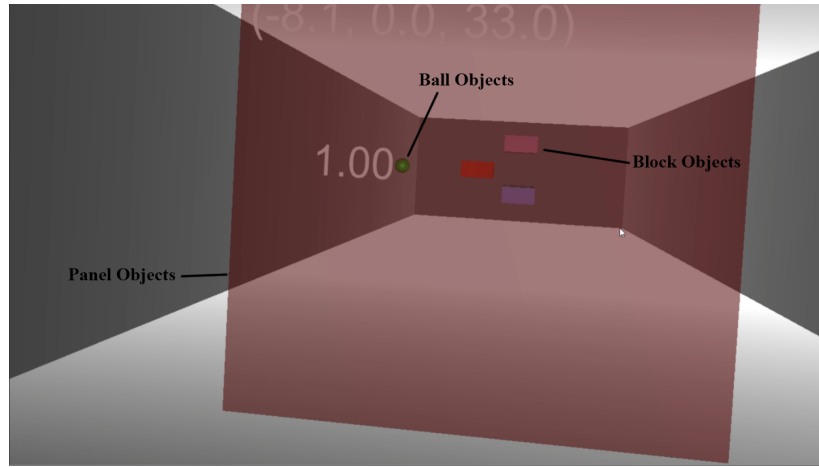


Figure 3.21: Blockbuster game screen capture.

Blockbuster Game Objects System: The Game Objects System was the primary system to present the game. There were three sub-systems in this system, which were: Panel Objects, Ball Objects, Block Objects.

One of the Panel Objects was instantiated at the start of each level. This object's position was controlled by participants' head rotation through the Head Simulator and Ray Cast Components. It inherited the Unity physics, which let the Ball Objects bounce back without losing velocity.

One of the Ball Objects was also instantiated at the start of each level. It also inherited the Unity physics so it could interact with the Block Objects and Panel Objects. It would trigger the fail-action (loss score) and re-spawn if the participants failed to catch the ball with the panel.

Block Objects were instantiated continuously in a certain period during the game. If hit by the Ball Objects, it would despair and add trigger bonus-action (add score). Based on the game mode, it may also move towards the participants.

State Machine Controller: The State Machine Controller contains the states for this game. A snapshot was illustrated in figure 3.22.

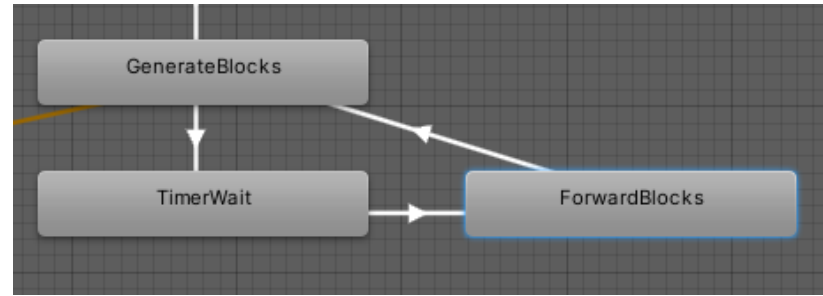


Figure 3.22: Blockbuster game state machine controller.

Generate Blocks: generate some blocks in the scene. Time Wait: wait for a certain period. Forward Blocks: move the blocks one step toward the participants.

Chapter 4

VOR Assessment Experimental Methods

4.1 Subjects

Six individuals (age 18-65) were recruited with written consent at the Louis Stokes Cleveland Dept. of Veterans Affairs Medical Center. All of the participants never had clinical histories of vestibular disorders. All participants participated in a protocol approved by the medical center's IRB.

4.2 Assessment Software Design

A novel, interactive VOR functional assessment interface, referred to as the assessment program, was developed to assess VOR function. The interface utilized data from head rotation, eye rotation, and the Xbox controller to evaluate visual acuity during VOR as a function of time using a calibrated, high pixel-density dual-monitor display.

4.2.1 General Assessment Experiment Paradigm

Figure 4.1 illustrated the general sequence through a single experiment session.

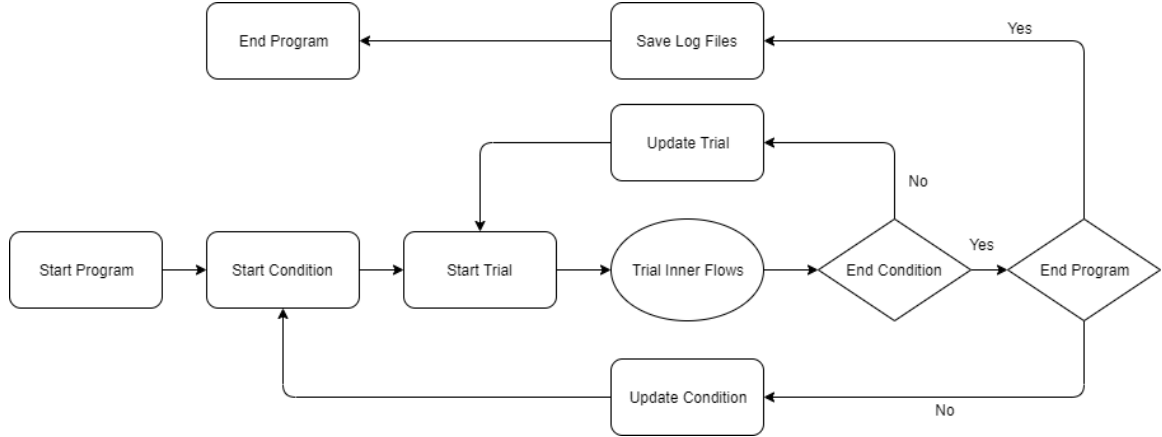


Figure 4.1: System General Flow Diagram.

Each square block represents an action conducted by the program. Each oval block represents multiple actions. Each diamond block represents a decisive action from the program. There were six conditions through an entire experiment, and once the program started, it loaded information and initiated the first condition. Each condition was separated into multiple trials, and information about all trial actions will be discussed through Section 4.2.2 to Section 4.2.6. Once the program covered all the trials in one condition, it updated the information of the next condition and started the next assessment. After finishing all conditions, the program would save all the log files and close automatically.

These six conditions were: static visual acuity (SVA) assessment, dynamic visual acuity (DVA) assessment, temporal dynamic visual acuity (TDVA) assessment, temporal gaze-shift visual acuity (TGVA) assessment, dynamic acuity head-eye rotation assessment, and gaze-shift acuity head-eye rotation assessment.

4.2.2 Static Visual Acuity Assessment

This is the very first condition of the entire experiment session for each participant. The purpose of this condition is to assess the visual acuity of the participants when the head is not rotating, referred to as static acuity (see Section 2.3). Participants were instructed to maintain their head and eyes in the forward direction for the duration of this assessment. Their head rotation data and Xbox controller inputs were recorded. The procedural steps of this condition are illustrated in the flow diagram in Figure 4.2. The Oval Shaped blocks represent multiple actions from the software, while the square blocks represent one single action. The diamond-shaped blocks represent the decision actions from the software.

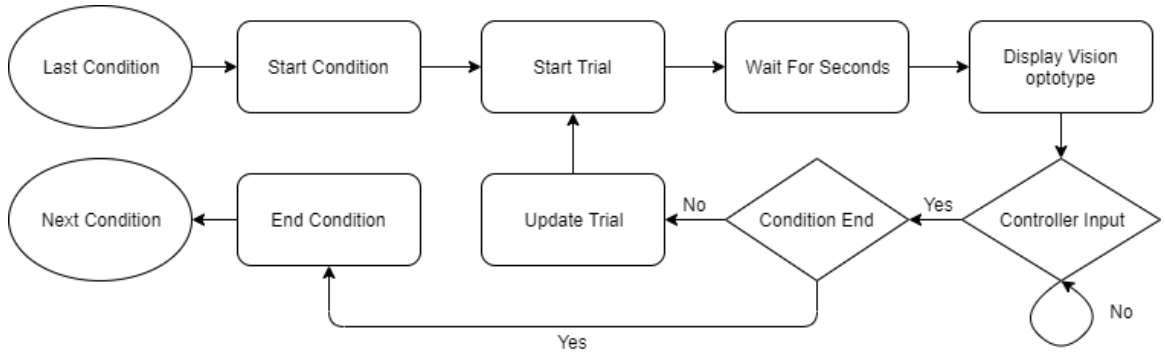


Figure 4.2: Static Acuity Flow Diagram.

As mentioned earlier in Section 4.2.1, there were actions before and after this condition, and they were omitted to the “Last Condition” and ”Next Condition” illustrated in Figure 4.2. The method for updating the conditions is shown in Figure 4.1. Each trial consists of multiple actions and started from the ”Start Trial” action. For each trial, an optotype with the gap facing a randomly chosen direction from 8 directions, four orthogonal and four diagonal directions, was used. As mentioned in Section 3.1.2, there were ten test sizes in the program. However, we used the best PEST [55] method to find the psychometric thresholds, and not all the test size would be covered.

The best PEST method was discussed by Bach et al. about how to test patients' visual acuity with Landolt-C optotypes. Since the optotype can be possibly displayed in 8 directions, and only one direction can be chosen to resolve the optotype, the possibility that the participants answered the test with guessing was 0.125. The equation for the best PEST method mentioned in the paper is (4.2). The V represents the size of the optotype, and L_{V_0} represents the likelihood of the size V_0 . The basic idea is it would calculate all the possibilities based on the correctness rate and incorrectness rate for that size, and use the size with the highest possibilities as the next test size. We can decide the participant's acuity if the equation's results come up with the same size repeatedly.

They also used the resolving accuracy of 56.25% as the acuity threshold (as psychometric thresholds mentioned in the paper). The equation to calculate the threshold number is (4.1). The ideal is to calculate the average rate in regards of the guessing rate.

$$\frac{100\% - 12.5\%}{2} + 12.5\% = 56.25\% \quad (4.1)$$

$$L_{V_0} = \prod_i (p_{V_0}(V_i))^{n_{correct}(V_i)} \times (1 - p_{V_0}(V_i))^{n_{incorrect}(V_i)}$$

Where (4.2)

$$P_{V_0}(V) = 0.125 + \frac{1 - 0.125}{1 + (\frac{V_0}{V})^S}$$

Once a trial started, the program waited for one second to let participants get prepared and then displayed the optotype for 80 ms. Once the participant's input from the Xbox controller was received, the input would be stored in memory. After each trial, the program would run the best PEST equation and decide which size to use as the test condition. If the equation produced the same answer for three

continuous trials, the program would terminate the condition.

The participants need to conduct two steps to input the gap direction with the Xbox controller. In the first step, participants need to push and hold the joystick (see Section 3.1.1) to the expected direction, while a Controller Indicator (see Section 3.1.2) would tell them which direction the joystick was pushed. Then, by pressing the shoulder button, they would confirm the direction they chose. The rationale for this two-step mechanic was to minimize the likelihood that participants would accidentally input the wrong direction on the first try.

The accuracy from a single size would be calculated by the Equation (4.3). The "C" represents the number of trials that the participants correctly resolved for a specific size, while the "N" represents the total trial numbers that had been conducted in this size.

$$Accuracy = \frac{C}{N} \quad (4.3)$$

4.2.3 Dynamic Visual Acuity Assessment

The purpose of this dynamic acuity assessment was to assess the participants' visual acuity during head rotations (see Section 2.3) toward the right and left directions separately. As detailed in the Background chapter, 2.2, vestibular dysfunction might affect the left and right vestibular canals to different degrees and thus need to be assessed independently. There were two conditions provided for this assessment, one for leftward head rotations and one for rightward head rotations. The first condition required participants to turn their head to the left side for testing, while the second required them to turn to the right side. Both of these conditions share the same procedure, shown in Figure 4.3.

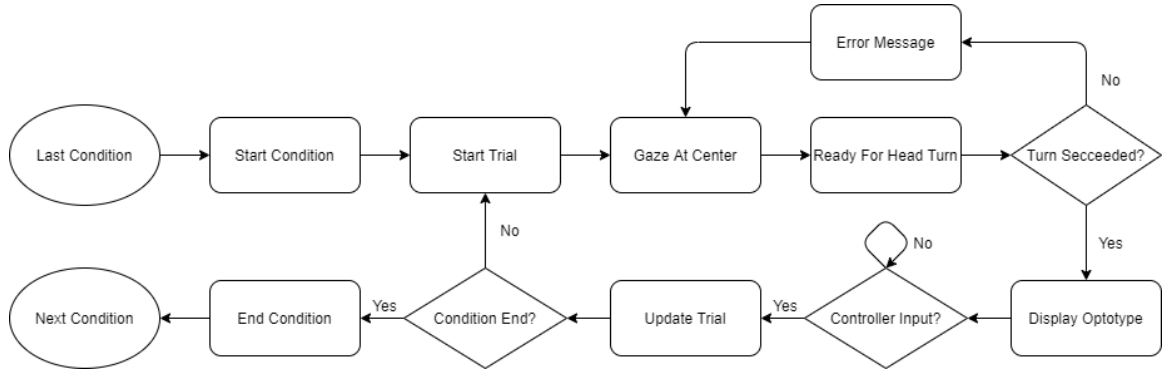


Figure 4.3: Dynamic Acuity Flow Diagrams.

Similar to the static acuity assessment, there were ten optotypes of different sizes (size indexes from 0 to 9, Section 3.1.2) prepared, and the best PEST equation would decide which size to use. Also, for each optotype, there were eight possible directions it would face toward, and each optotype was presented for 80 ms.

The general assessment flows also illustrated in Figure 4.4. There were two significant steps in this assessment and were marked as “1” and “2” in Figure 4.4.

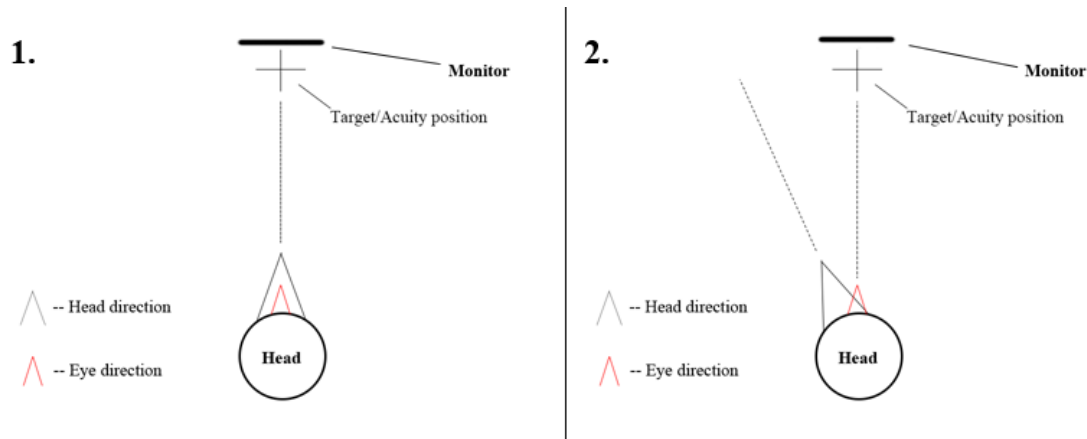


Figure 4.4: Assessment Flows of Dynamic Acuity.

At the start of each trial, the participant was asked to center their head to the forward direction to prepare for the turning, refers to Figure 4.4 step 1. This is defined as the Natural Head Position (rotation of zero for all axis), and all the other rotation will be calculated relative to this rotation. Notice that the magnetic field system and

the Simulink program could not automatically detect the Natural Head Position since it was different among all participants. Thus, manual actions were required from the staff to set the Natural Head Position correctly (see Section 3.1.2). During this step, a centering Target Indicator (see Section 3.1.2) was displayed on the monitor. Once participants reached the center target, the program would display a signal to instruct the participant to turn their heads. Then, it monitored the head's angular velocity and judged whether the head-turning was valid, which was discussed in Section 3.1.2. If the velocity was too slow or in the wrong direction, an error message was displayed to inform the participants and prompt the participants to restart the trial. When the head-turn was valid, an optotype was displayed for 80ms in the center of the monitor, illustrated in Figure 4.4 step 2, and the participants need to resolve the direction the optotype faced and use the Xbox controller to input the orientation they perceived. All the head-turn data and Xbox controller inputs were logged into files for later analysis.

4.2.4 Temporal Visual Dynamic Acuity Assessment

The purpose of this assessment was to get the data of the amount of time after head rotation started that allows participants to most accurately resolve the optotype symbol, which was referred to as re-fixation time. This assessment focused on the VOR only affected head-eye rotations (only one focus position was provided during the head movement). The condition was referred to as a temporal dynamic acuity assessment. As discussed in Section 2.4, human eyes act differently during different stages of the head-turning process. To assess the re-fixation time, the program waited a certain amount of time at the beginning of the head-turning process and displayed the optotype after the waiting. This assessment would then combine head-turning data with the delayed acuity correctness rate and found the relationships between them. The leftward head rotations were tested first, followed by rightward head

rotations. During the entire assessment, the optotype size was kept constant at one index larger than the smallest size resulting from the first static acuity condition (see Section 4.2.2). The rationale for this was that temporal dynamic acuity should be the same as static acuity when the delay was long enough. Effectively, participants will have finished the head-turn before the optotype was displayed, and reading the optotype will have occurred when the head's rotation speed is at a minimum.

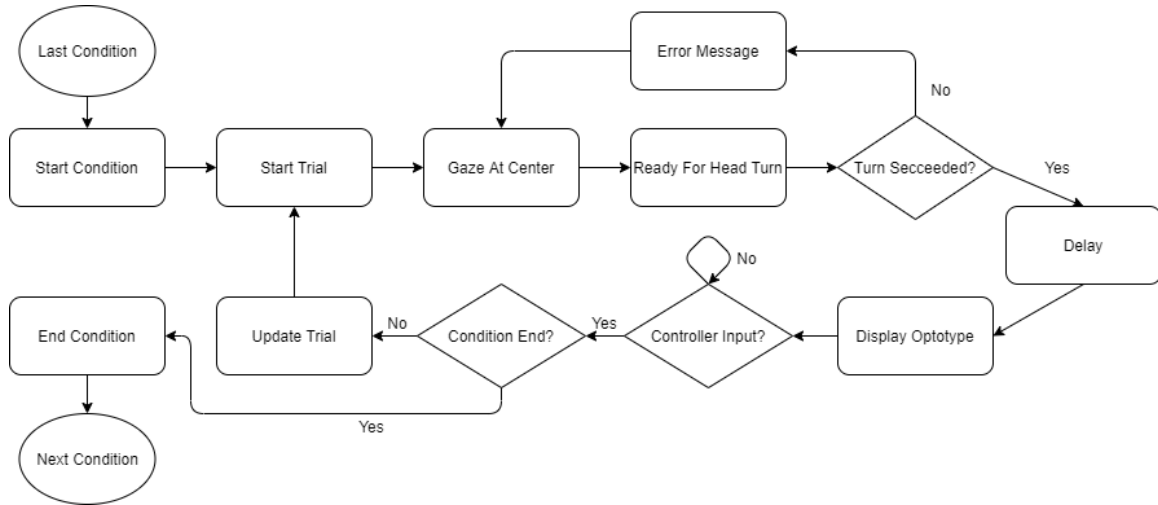


Figure 4.5: Temporal Dynamic Acuity Flow Diagram.

The procedure for this condition is illustrated in Figure 4.5. The flow diagram for this condition was very similar to the dynamic acuity assessment. As a trial started, participants were required to gaze at the monitor's center. After, a signal would prompt participants to turn their heads either to the left or right sides. Once the head-turn succeeded, the program will wait for a certain amount of time before displaying the 80 ms optotype. There were ten different delay periods used, and each of them was repeated for nine trials to get enough data. The first delay was 0 ms, which means no delay, and after nine trials, the delay time was increased by 80 ms, up to the maximum delay time 720 ms. Then, after reading the optotype, the participants need to input the response with the Xbox controller. All the head-turn data was recorded, as well as the Xbox controller response actions, and was

written to files for later analysis. Also, A judgment implemented in the program allows it to end this condition before the delay period reached 720 ms, so the entire experiment would not be too long. If the participants could resolve 77.8% (7 of 9) of the optotypes for the current delay period correctly and their head-turn processes ended before the optotype was displayed for each trial, we defined this as the point at which the participants have reached the passing threshold for this condition and no further tests in this condition were needed.

4.2.5 Temporal Gaze-Shift Visual Acuity Assessment

Similar to the Temporal Dynamic Visual Acuity condition, the purpose of this assessment was also to get visual recovery time. However, instead of a single target position as temporal dynamic visual acuity condition used, this condition assessed the data during the rapid eye movement that occurs when changing the object of visual fixation from one location to another, referred to as a gaze shift (see Section 2.4). In this condition, we would rotate the participants' chairs so that their Natural Head Position (see Section 4.2.3) was pointed to the center of the dual monitor system. Unlike assessing dynamic acuity, which required participants to start from the forward-facing direction, participants were told to follow a Target Indicator (see Section 3.1.2), that were displayed alternatively either to the left or right side monitor to simulate a gaze shift. Similar to the prior condition, optotypes were presented with time delays to measure visual acuity re-fixation time. The one index larger than the minimum static acuity size from the Static Visual Acuity Assessment condition was used for this entire assessment as well. Also, with the Target Indicator appearing on the left and right monitors sequentially, it was unnecessary to separate the left and right assessments into two assessments. The total number of trials was 180, including 90 presentations of the optotype on the left monitor and 90 on the right monitor. The passing-threshold (see Section 4.2.4) was also implemented in this condition. The

procedural flow diagram is illustrated in Figure 4.6.

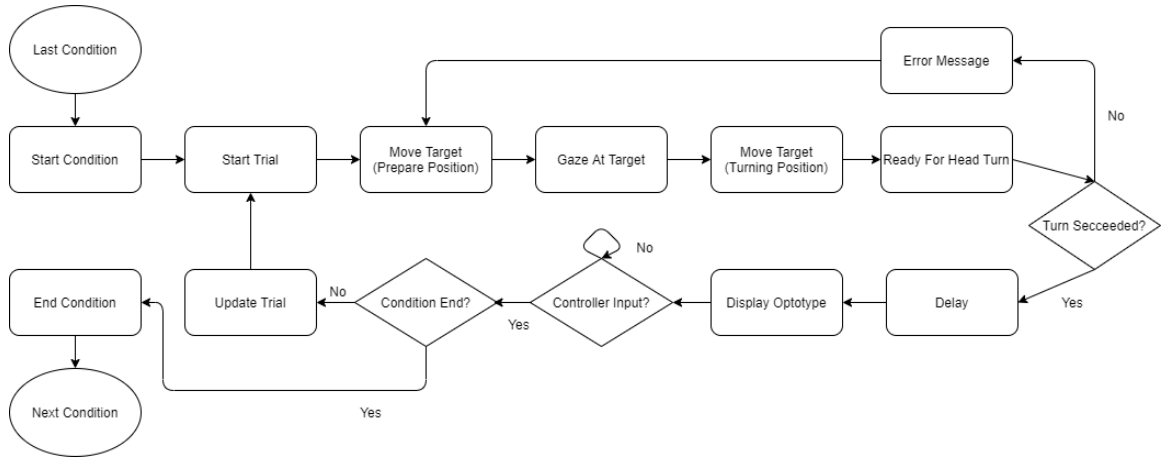


Figure 4.6: Temporal Gaze Flow Diagrams.

Figure 4.7 showed a general assessment flows of this condition. There were primarily three steps in this assessment, marked as “1”, “2” and “3”, and the fourth step showed the starting step of next trial (similar to the step 1 and 2), but on the opposite direction.

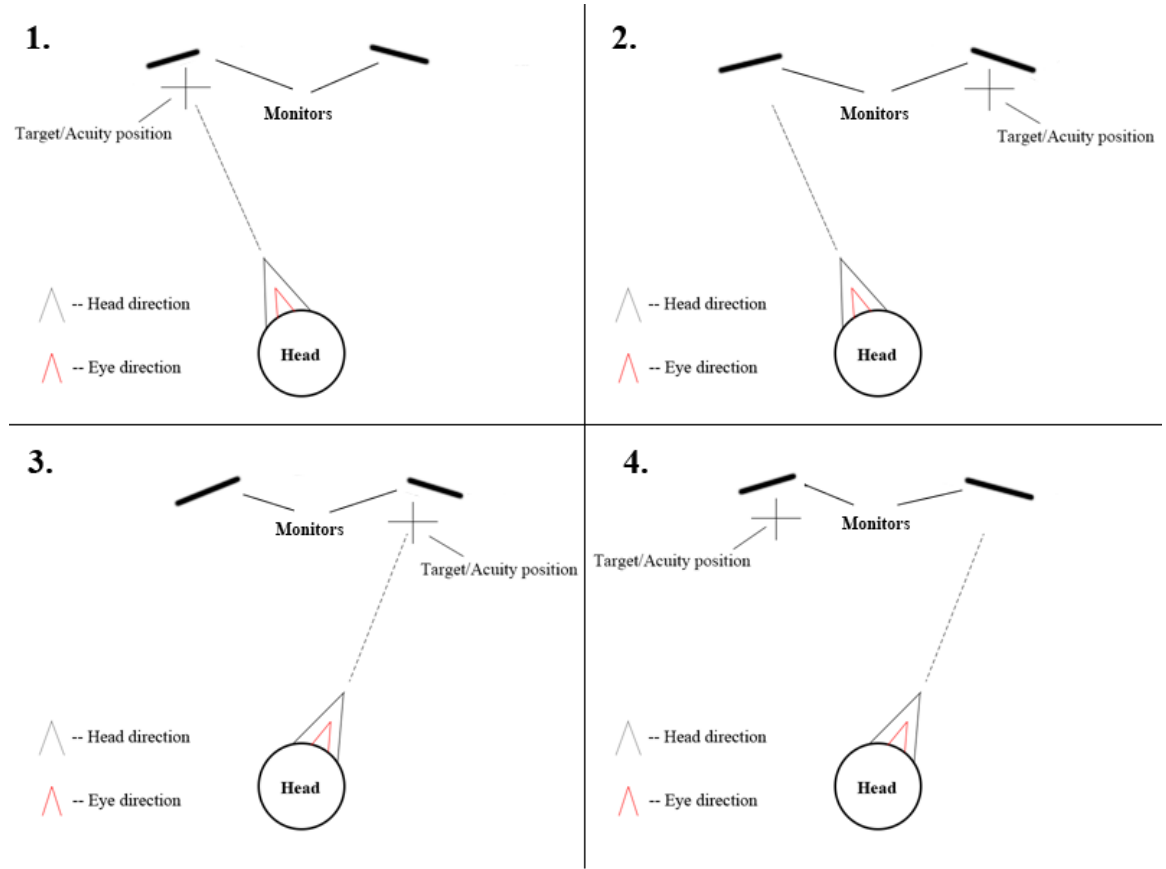


Figure 4.7: Temporal Assessment Flows of Gaze Shift.

Similar to the Temporal Dynamic Acuity Assessment condition, there were ten different time delays, starting from 0 ms to 720 ms. Each delay was repeated for nine trials for both left and right side targets, which resulted in 18 trials for each delay. When a trial started, the program would put the target on the left or right monitor and instruct the participants to turn toward the target, see Figure 4.7 step 1. There were two positions defined in each trial, preparation position, and turning position. At the start of the gaze shift, the preparation position was used to lead the participants to focus on before the head-turn. The turning position indicated the stop position of the head-turn. Both target positions were pre-defined to be 35 degrees of angular distance on the Natural Head Position's right or left position. This results in 70 degrees of head rotations for both the left and right head-turn directions. After

the participant reached the preparation position, the target appeared at the turning position and waited for the participants to turn their heads, referred to in Figure 4.7 step 2. As usual, there would be a judgment about whether this head-turn process was valid (see Section 3.1.2). If it was valid, the optotype was displayed with a delay at the target position (Figure 4.7 step 3). Participants were tested whether they could see the target direction during and after a natural gaze shift. If the head-turn process failed, the Target Indicator moves back to the preparation position, and the participants need to redo this trial. All the head rotations and controller inputs were recorded and written into files for offline analysis.

4.2.6 Temporal Assessment With Eye Data

In these assessments, the purpose was not to assess visual acuity but to obtain eye and head rotations data only. Since we do not need to calculate visual acuity, each delay was only repeated three times for a total of 30 trials. Both temporal dynamic acuity assessment and temporal gaze shift assessment were conducted, and all the condition procedures were kept consistent except the trial numbers. The head rotation data and eye rotation data were recorded and written into files for later analysis.

Chapter 5

Results

5.1 Static Visual Acuity Assessment

As detailed in Section 4.2.2, static visual acuity quantifies a person’s best vision when the head is still. Here it provides a baseline against which DVA (see Section 4.2.3), TDVA (see Section 4.2.4), and TGVA (see Section 4.2.5) can be compared.

Figure 5.1 shows an example of one subject’s static visual acuity. To better visualize the data, we used a logistic function $f(x) = \frac{L}{1+e^{-k(x-x_0)}} + 0.125$ and feed the x (optotype size) and $f(x)$ (accuracy of the responses) data to form the curve. As stated in Section 4.2.2, static visual acuity was tested using optotypes of ten sizes, but the best PEST equation would decide which size to use. All the dots in the figure represents the test results from this condition. The x-axis represents the optotype sizes in logMAR equivalent (see Section 2.3). The y-axis represents the results (accuracy of the responses) from the subject. Each optotype size may repeat multiple times, and the number that subjects answered correctly for each size divided by the total number tested for each size was defined as the accuracy of the responses (AOR). The dotted line represents the AOR of 56.25%, and the rationale of this was illustrated in Bach’s paper [55]. (see Section 4.2.2)

As shown in Figure 5.1, this subject has low AOR when the optotype is very small (logMAR of -0.182), but as the optotype gets larger (after logMAR of 0.232), the AOR increases to 63.6%.

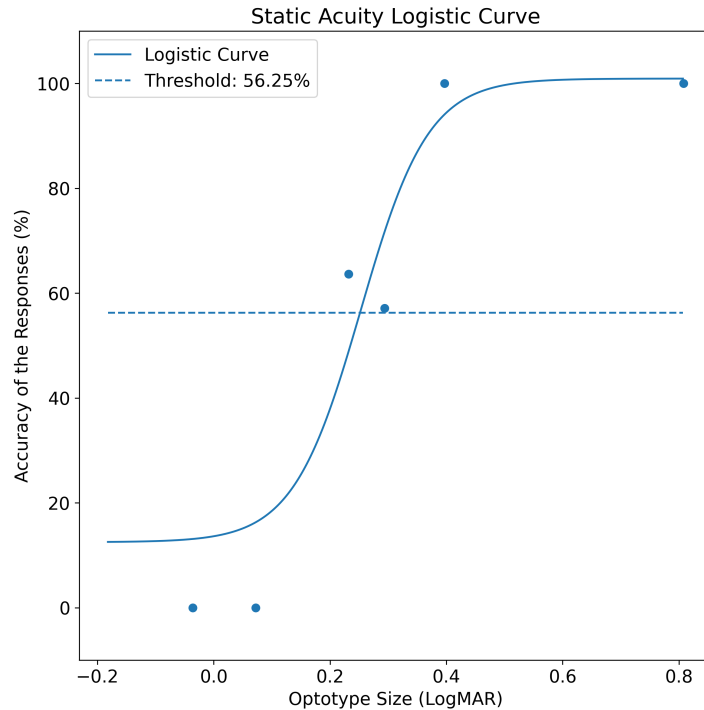


Figure 5.1: Static visual acuity results after curve fitting, for a single participant, the x-axis represents the optotype size presented during the experiment, and the y-axis represents the accuracy of the participant resolving these optotypes. The Threshold line is drawn at the accuracy of 56.25%. The logistic curve equation.

Based on the best PEST method, this subject's static acuity is 0.232 logMAR. It suggests that the subject has a SVA of 20/34 in Snellen (see Section 2.3).

As shown in Figure 5.2, all of six subjects' SVAs are under 0.3 logMAR (with or without corrective glasses) during the experiment. The median SVA was 0.137 logMAR.

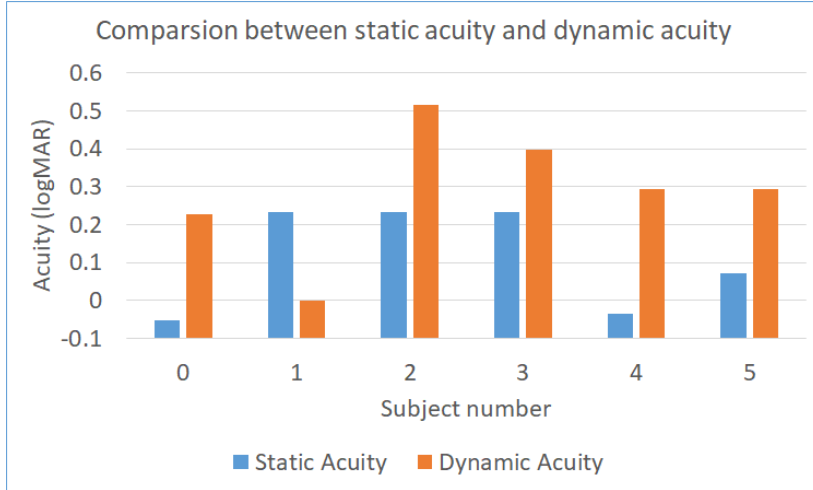


Figure 5.2: Comparison between SVA and DVA for all subjects. Larger logMAR indicates worse acuity.

5.2 Dynamic Visual Acuity Assessment

Dynamic visual acuity quantifies a person’s best vision while head is rotating, which is related to the functionality of VOR (see Section 2.3). We hypothesize that the program could test the visual acuity similar as other methods, which means that the result that from this measure program would match other literature (see Section 2.3) that the DVA of able-bodied participants should be slightly greater than their SVA since people usually do not have perfect VOR (as higher logMAR values means a participant is able to resolve a larger optotype, which equates to reduced visual acuity).

The Figure 5.3 shows an example of the same subject’s logistic fit from which dynamic acuity is derived. The DVA condition used ten optotype sizes, and the best PEST method was also used. As shown in the figure, the subject’s performance improved when the sizes got larger, and the highest AOR was 100%.

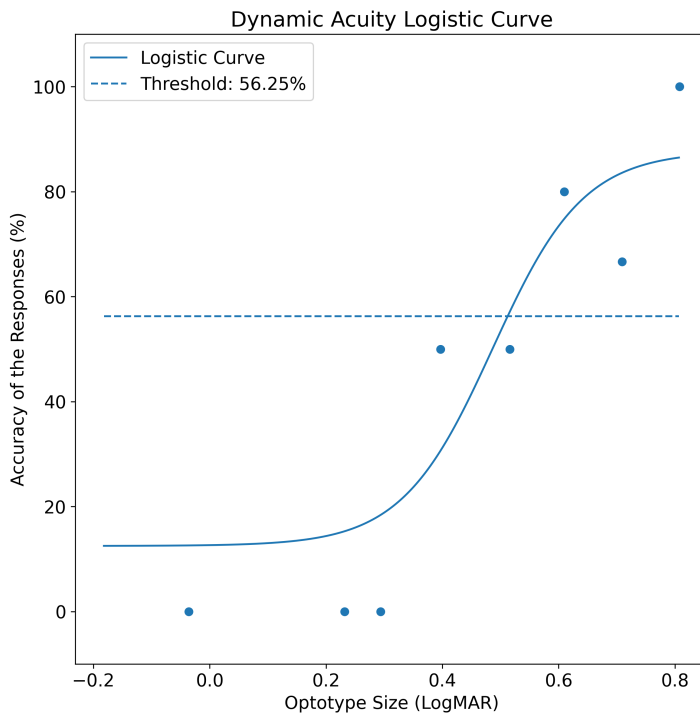


Figure 5.3: Dynamic visual acuity result after curve fitting, from a single participant. The x-axis represents the optotype size presented during the experiment. The y-axis represents the accuracy of the participant resolving these optotypes. The Threshold line was drawn at the accuracy of 56.25%.

The subject's DVA was 0.516. Compared to the subjects SVA of 0.232, the subjects' DVA was worse than his SVA.

The Figure 5.2 also shows dynamic acuity for all subjects.

Three of five subjects' dynamic acuity were smaller than 0.3 logMAR. The median DVA was 0.294 logMAR. As expected, five of six subjects show that their DVA is worse than their SVA.

5.3 Temporal Dynamic Vision Acuity Assessments

The procedure of the Temporal Dynamic Vision Acuity assessment is discussed in Section 4.2.4. Basically, the optotypes' presentation on the monitor is delayed for a certain time after the start of the head-turn. The primary measurement is the temporal DVA (TDVA), which is the DVA that related to the optotype delay time. An example of the TDVA is illustrated in Figure 5.4.

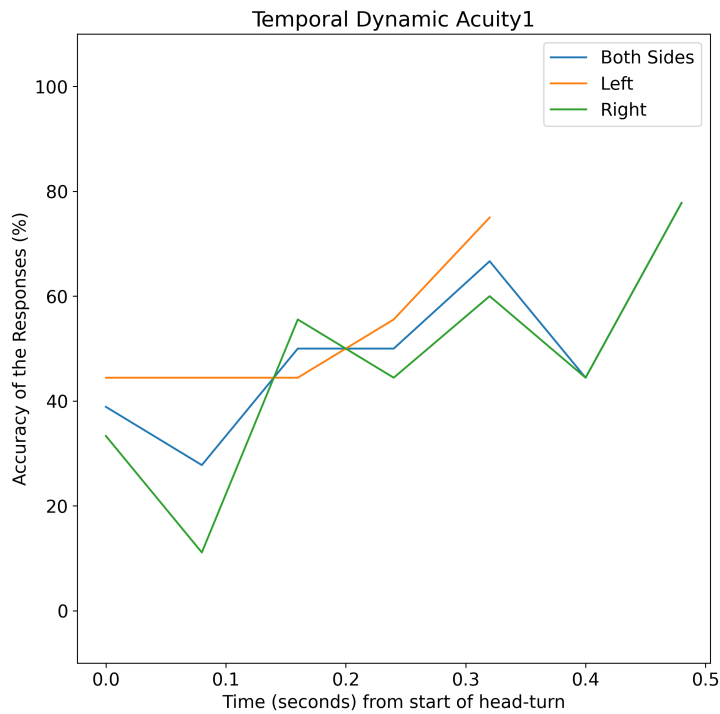


Figure 5.4: Temporal dynamic visual acuity result from a single participant. The x-axis represents the time in seconds that had been delayed before presenting the optotype. The y-axis represents the accuracy of the participant resolving these optotypes. Both left-side turn and right-side turn results were shown in the figure. The combination of left and right head rotation trials is presented as “Both Sides”

The x-axis represents the time delay in seconds relative to the start of the head-

turn. As discussed in Section 4.2.4, there are ten delay periods tested. The AOR from each delay time was calculated and the overall AOR is plotted on the figure. Usually, people with healthy VOR will have similar performance for both left and right direction head turns. However, people with vestibular dysfunction may have different performance for left and right direction head turns (see Section 2.2), so we also analyzed the left and right head-turns separately, refer to as the line “Left” and “Right” in Figure 5.4. The combination of the left and right directions is referred to as total TDVA and is shown using the blue line labeled “Both Sides.” We used the acuity size of logMAR 0.072 as the test size for this participant while the participant’s static acuity is logMAR of -0.036. The AORs for left and right head turns are different but with a maximum of 30% AOR difference. The average difference is 11.8%.

The Figure 5.5 shows both sides Temporal Dynamic Acuity for all subjects.

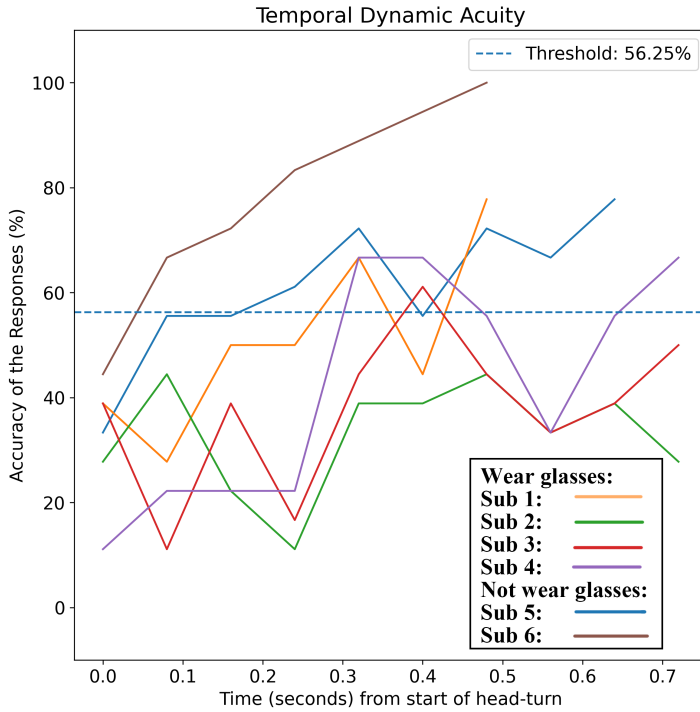


Figure 5.5: Temporal dynamic visual acuity results, from all the participants. The x-axis represents the time in seconds that had been delayed before presenting the optotype. The y-axis represents the accuracy of the participant resolving these optotypes.

Five of six subjects were able to resolve the optotype with an accuracy above the threshold (AOR 56.25%). Their patterns were not consistent because people who wear glasses may have different vision during the test (see Section 6.3). Four of the six subjects showed increasing patterns with the delay period.

5.4 Temporal Gaze-shift Acuity

The procedure of the Temporal Gaze-shift Acuity is described in Section 4.2.5. The subjects were instructed to conduct similar head rotation to the TDVA tests, while

this time, their eyes were instructed to focus on the target that may change positions on the screen. This aimed to simulate the gaze-shift that occurs when looking around the world in daily life (see Section 2.4). One of the examples is shown in Figure 5.6.

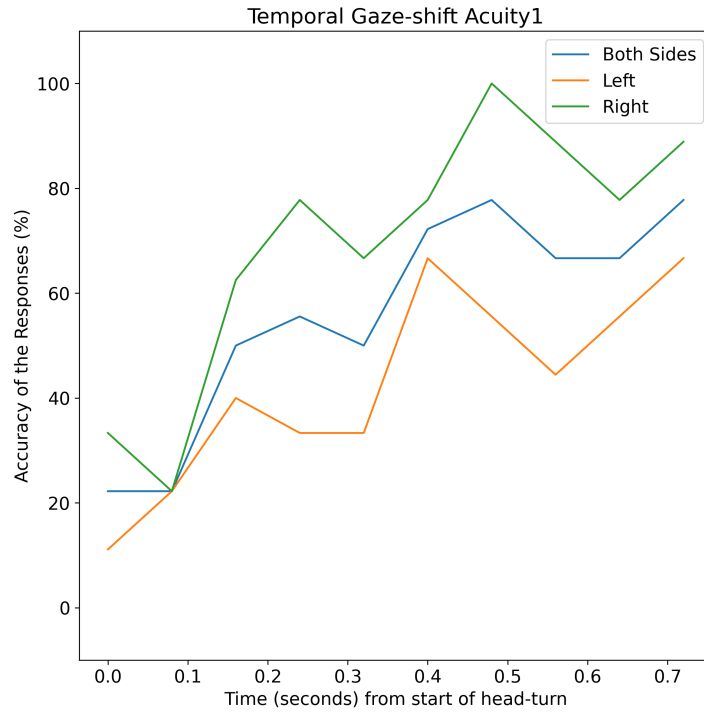


Figure 5.6: Temporal gaze-shift visual acuity results, from a single participant. The x-axis represents the time in seconds that had been delayed before presenting the optotype. The y-axis represents the accuracy of the participant resolving these optotypes.

Similar to the TDVA, both left and right head rotations were analyzed in this task. The x-axis represents the time in seconds that delayed from the start of the head-turn, and the y-axis represents the AOR for each delay period. The AOR increased as the delay time increased. Since the total TGVA is increasing with the delay period, we used the same logistic equation detailed in Section 4.2.2 and found the logistic curve to of this subject, which is shown in Figure 5.7.

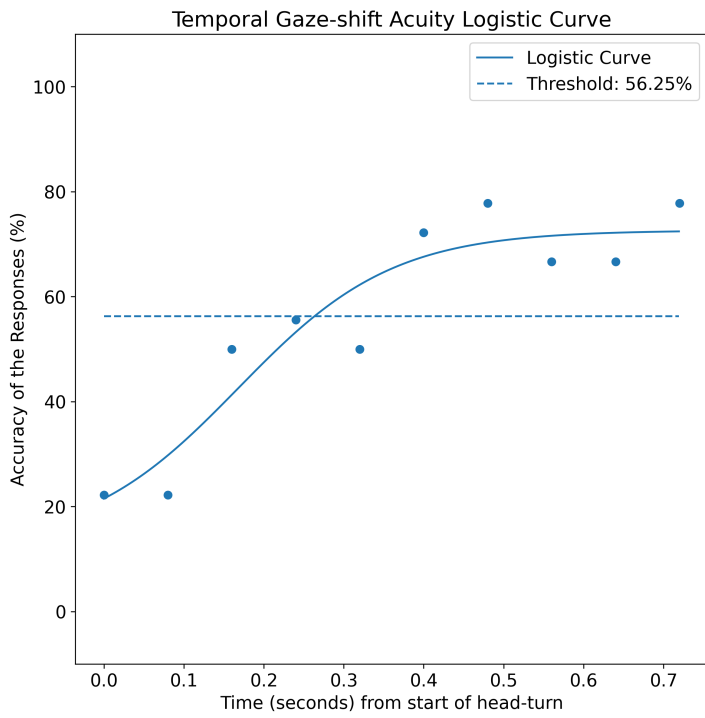


Figure 5.7: Temporal gaze-shift visual acuity results after curve fitting, from a single participant. The x-axis represents the time in seconds that had been delayed for being delayed before presenting the optotype. The y-axis represents the accuracy of the participant resolving these optotypes.

From the curve in Figure 5.7, we concluded that this subject passed the threshold at the delay period of 260 ms. To analyze the whole group, we plotted the logistic curves for all the subjects and illustrated them in Figure 5.8.

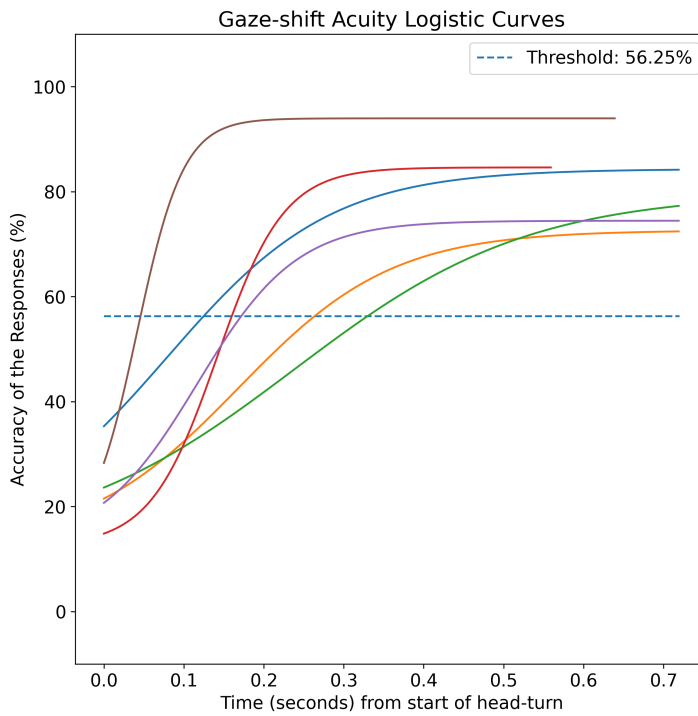


Figure 5.8: Temporal gaze-shift visual acuity results after curve fitting, from all participants. The x-axis represents the time in seconds that optotype presentation had been delayed. The y-axis represents the accuracy of the participant resolving these optotypes.

All the subjects share the same pattern that AOR is increasing with the delay period. Four of the six subjects' re-fixation time for gaze-shift was smaller than 0.2 seconds, and all subjects' re-fixation time was smaller than 0.35 seconds. The median re-fixation time is 0.160 seconds.

5.5 Head-turn trajectory measurement

We recorded the velocities of the head, eye, and gaze for all the subjects with the pupil tracking glasses and the coil system for both Temporal Dynamic Acuity tasks

and Temporal Gaze-shift Acuity tasks (see Section 4.2.6). An example of the head-eye rotation trajectory during the dynamic acuity task is illustrated in Figure 5.9. Subplot A shows a single trial, and subplot B shows multiple trials.

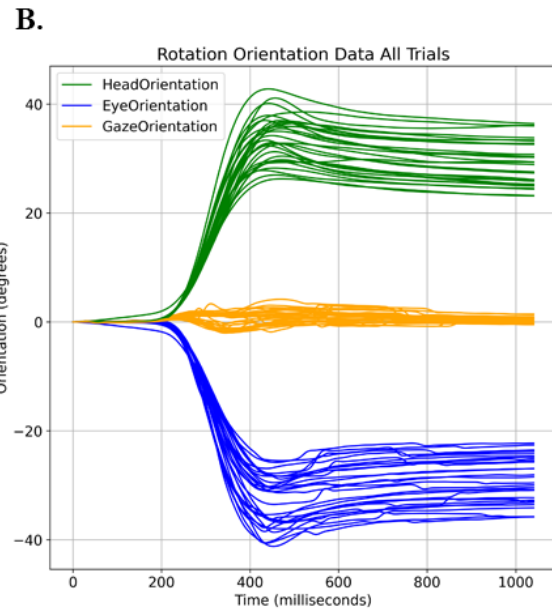
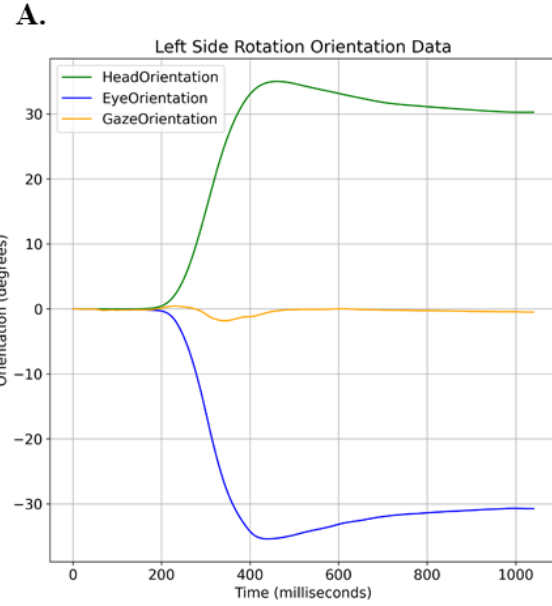


Figure 5.9: Orientation data of head, eyes, and gaze during head rotation in temporal dynamic visual acuity task from a single participant. Subplot A shows an example of a single trial, subplot B show multiple trials. The x-axis represents the time in milliseconds. The y-axis represents the orientation in degrees, left as positive

The y-axis represents the orientation in degrees, in which left-side orientation is

represented in positive numbers, and right-side orientation is represented in negative numbers. The head orientation that was recorded from the coil system, which is relative to the Natural Head Position (see Section 4.2.3), is represented as the green lines labeled “Head Orientation.” The eye orientation relative to the head orientation, which was recorded with pupil tracking glasses (see Section 3.1.1), is represented as the blue lines. The combination of the previous two, which is represented as the yellow lines, shows the subject’s gaze orientation relative to the Natural Head Position. In the TDVA tasks, the subject will be instructed to fix their eyes and head to the Natural Head Position, which refers to at the timestamp of 0 ms as both head’s and eyes’ orientation were nearly zero degrees. In subplot A, at 200 ms, this subject started to turn their head to the left side. Since the participant was instructed to fix the gaze on a target showing on the screen, which, in this situation, is located at the Natural Head Position, this subject started to turn eyes to the right side to compensate for head rotation to the left. At around 400 ms, the subject finished the head-turn motion and stayed in this position for a while, although there was little reverse turning shown on the figure. As we can see from the subplot A, this subject was able to, though not perfectly, fix the gaze at the Natural Head Position during the head-turn motion. The gaze orientation was shifted less than three degrees, which suggests that the participant had a functional VOR. However, since the gaze orientation is still not perfectly fixed, this subject could still experience blurred vision during the head-turn.

For the purpose of analyzing the consistency of this head-turning trajectory, subplot B shows multiple trials. It shows 29 trials of the head-eye rotation trajectory for the Temporal Dynamic Acuity task. There are a total of 30 trials recorded (see Section 4.2.6). However, some trials may contain errors, either from sensors, such as lost tracking or noise, or from the subject’s actions, such as blinking. Thus, sometimes we need to discard some trials if they contain too many errors. Even so, the

error occurred only once during the experiment shown in this figure, so one trial was discarded in this situation. Also, subjects may turn their head to either left or right side, but it is inconvenient to analyze the consistency with two different direction lines. Thus, we inverted trajectory data from the right-side head-turns. We can see that from all those trials, the lines are mostly following the same pattern, despite different maximum rotation angles (ranged from 25 degrees to 43 degrees). The eyes are counter-rotating against the head from the start of the head-turn to the end, and all the trials show a small amount (maximum of 5 degrees) of gaze shifting during the head-turn. The average trajectory data for the trials from Figure 5.9 is shown in Figure 5.10.

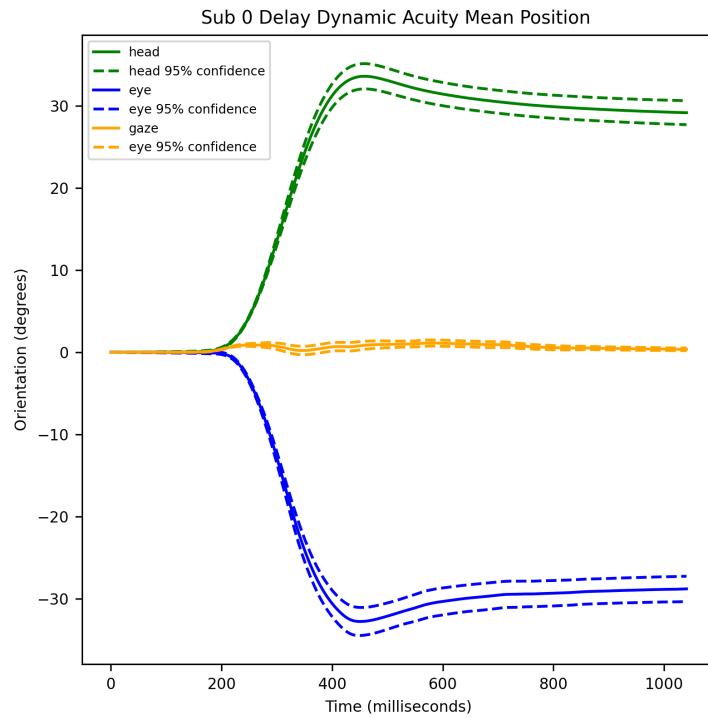
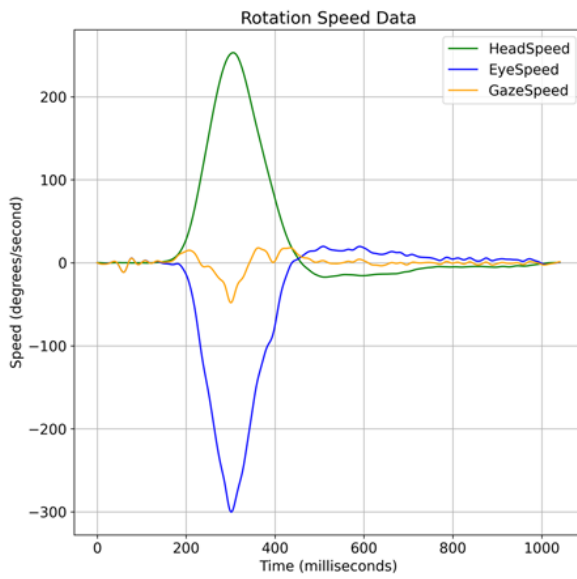


Figure 5.10: Average orientation data of head, eyes and gaze during head rotation in temporal dynamic visual acuity task, from a single participant. The x-axis represents the time in milliseconds. The y-axis represents the orientation in degrees, left as positive

The solid lines represent the mean trajectory, and the dashed lines represent the 95% confidence limits of the mean trajectory. As we can see, the variance gets larger after the beginning of the head-turn, as participants may turn their heads to different maximum angles each trial.

We measured the gaze-shift speed to determine the severity of vision blurring since greater speed implies more blurring. Figure 5.11 shows the velocity data of the same participant shown in Figure 5.9, subplot A shows a single trial same as shown in Figure 5.9, and subplot B shows multiple trials.

A.



B.

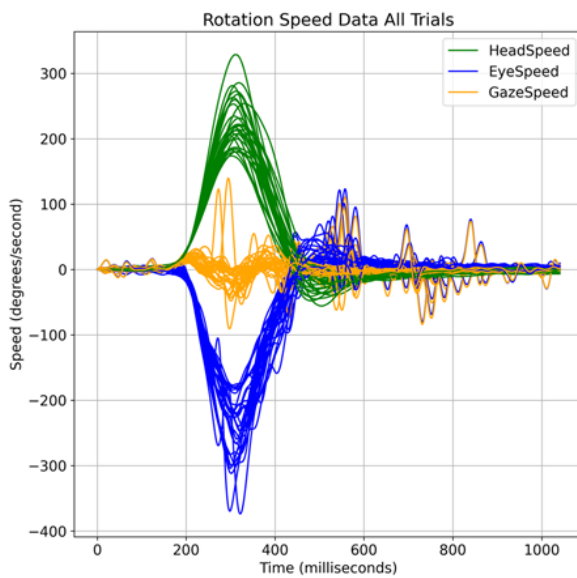


Figure 5.11: Angular velocity data of head, eyes, and gaze during head rotation in temporal dynamic visual acuity task, from a single participant. Subplot A shows an example of a single trial. Subplot B shows multiple trials. The x-axis represents the time in milliseconds. The y-axis represents the velocity in degrees per second, left as positive

From subplot A, we found out that during the head-turn motion (200 ms to 400 ms), the gaze rotational speed does not remain constant for this trial, which confirmed our suspicion that the subject is experiencing blurred vision at these delays. The maximum rotational gaze speed is -43 degrees per second. The gaze speed went back to zero again when the head and eye speed back to zero, which implies this subject was able to achieve visual stability after this point, referred to as the re-fixation point. The time from the start of the head-turn to the re-fixation point is 290 ms, referred to as re-fixation time from the start. The time from the end of the head-turn to the re-fixation point is 20 ms, referred to as re-fixation time from the end. We analyzed other trials and found this pattern to be consistent in all trials.

In subplot B, We can see that although maximum speed is not the same for each trial (head ranged from 210 to 330 degrees per second, eye ranged from 245 to 375 degrees per second), the pattern of both the head speed trials and eye speed trials are similar. All the trials (both left and right side rotation) showed that there was rotational gaze speed during the head-turn motion. The maximum gaze speed is 140 degrees per second among these trials. The average speed is shown in Figure 5.12.

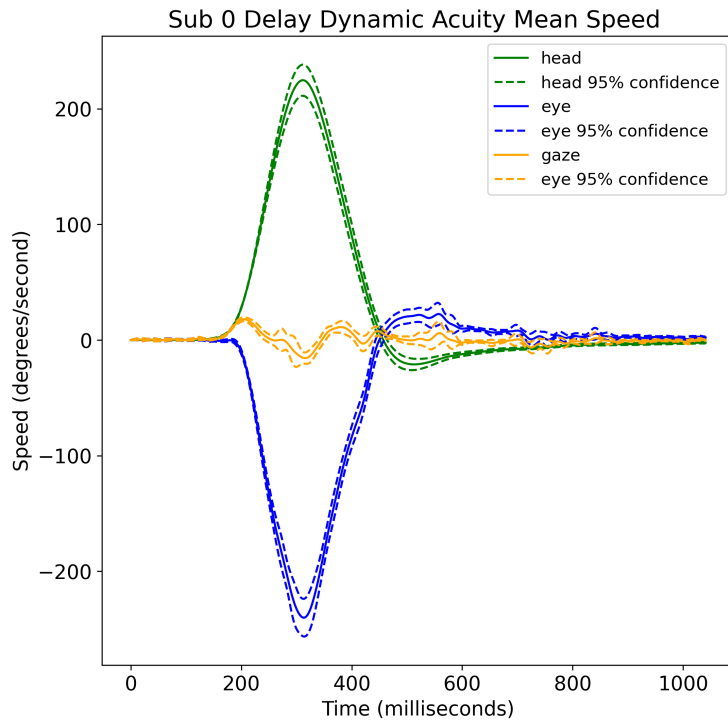


Figure 5.12: Average angular velocity data of head, eyes and gaze during head rotation in temporal dynamic visual acuity task, from a single able-bodied participant. The x axis represents the time in milliseconds, y axis represents the velocity in degrees per second, left as positive

We see the maximum variance of the speed for the head, eye, and gaze coincided with their maximum velocities. The average maximum gaze shifting speed is 18 degrees per second.

To analyze the relationship between the head-eye rotation pattern and the TDVA, we combined the trajectory data from the Section 5.2 with the orientation and speed data above, shown in Figure 5.13.

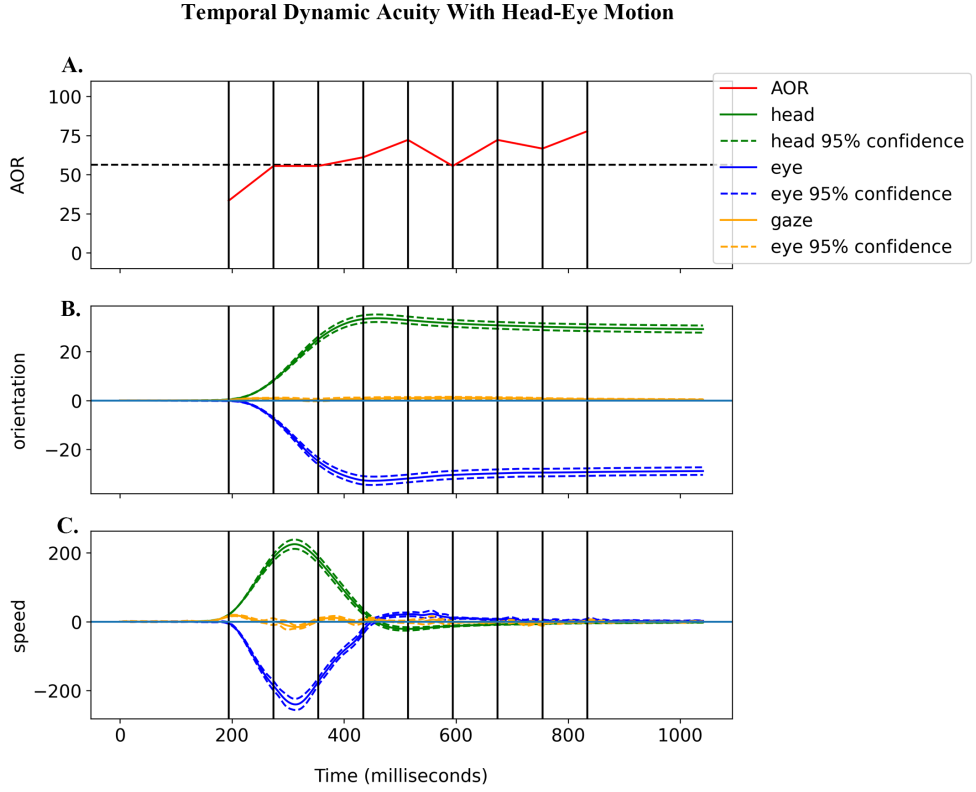
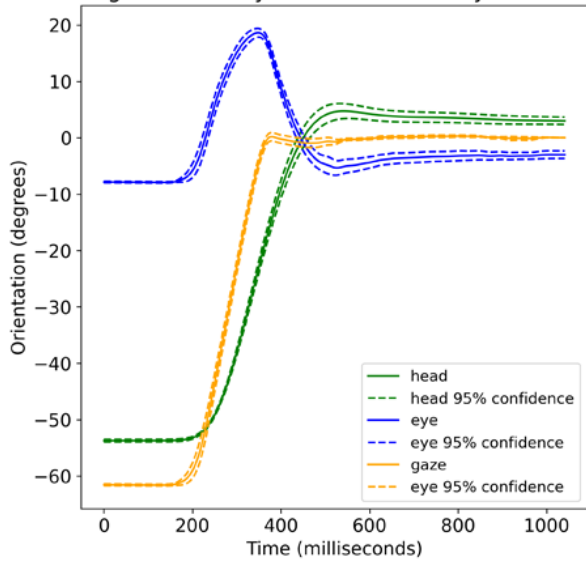


Figure 5.13: Combination of the TDVA task from a single subject. Subplot A shows AOR of temporal dynamic visual acuity. The y-axis represents the AOR. Subplot B shows orientation data of the head, eyes, and gaze. The y-axis represents the orientation in degrees. Subplot C shows angular velocity data of the head, eyes, and gaze. The y-axis represents the velocity in degrees per second. Shared x-axis: time in milliseconds.

The subplot A in the figure shows the TDVA for this subject, and the orientation and speed are plotted in the subplot B and C. Since these data were not simultaneously recorded (see Section 4.2.6), we aligned them using timestamps. The first point (vertical bar) from subplot A represents the delay period of 0 ms, which means at the very beginning of the head-turn. To find this point, we set a threshold of 5 degrees per second of the head rotation speed and defined that point as the beginning of the head-turn. The time interval of each point in subplot A is 80 ms.

A.
Sub 0 Right Side Delayed Gaze-shift Acuity Mean Position



B.

Sub 0 Right Side Delayed Gaze-shift Acuity Mean Speed

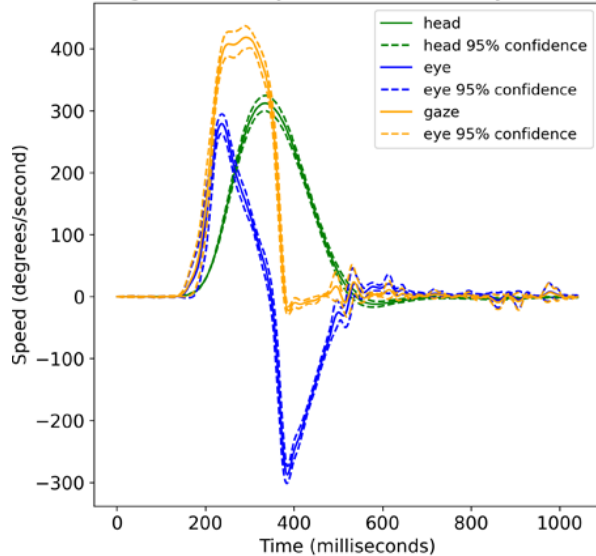


Figure 5.14: Data of head, eyes, and gaze during head rotation in gaze-shift visual acuity tasks from a single participant. Subplot A shows the orientation data, and subplot B shows the angular velocity data. The x-axis represents the time in milliseconds. The y-axis in subplot A represents the orientation in degrees. The y-axis in subplot B represents the angular velocity in degrees, left as positive.

We also analyzed these relationships for the gaze-shift tasks. The Figure 5.14 shows an example of the gaze-shift trajectory and velocity. This shows the average trajectory and velocity data for all trials of left-side head turns for one subject, subplot A shows the orientation, and subplot B shows the angular velocity. For subplot A, we defined the orientation angle that the participants were focusing on the left side monitor as the angle of zero degrees, which made the Natural Head Position located at around -35 degrees and the right side monitor located at -70 degrees. The subject was instructed to focus on a target displayed on the right side monitor, refer to the timestamp of 0 ms. The head orientation is nearly -63 degrees relative to the left side monitor, and the eye orientation was about 3 degrees relative to the head. This resulted in gaze orientation of around -60 degrees relative to the left monitor. Then, the target was moved to the left monitor, and the subject was instructed to move the gaze to the new target position. This occurred between 200-500 ms as the head orientation reached approximately zero degrees. In this figure, we can see the pattern while this subject conducts a gaze-shift task. When head-turn begins, this subject rotated the eyes and head to the target simultaneously, but the eyes were able to reach the target first at around 300 ms. Since the head is not at the ideal position yet, the subject kept rotating the head until to around zero degrees while keeping the gaze position on the target, which resulted in counter-rotating the eyes against the head rotation. At around 500 ms, the subject's head reached the target. The 95% confidence lines show that the greatest variation happened just before this subject stopped the head-turn motion and that eye rotation variance is larger than head rotation. After the head-turn, the subject may maintain their head and eyes in different orientations, but the overall gaze orientation is similar. For the angular velocity data in subplot B, we see that at around 200 ms, the eye speed and head speed started to increase simultaneously, but the eyes rotated faster. The maximum head speed is faster than the maximum eye speed, although the eye rotation speed

shows a more considerable variance than the head. The re-fixation point was located at around 400 ms when the gaze-speed dropped significantly, which implies that at this point, the subject should be able to maintain a relatively visual stability after the head-turn. To find the relationship between the head-rotation pattern with the TGVA, we combined the plots for this subject in Figure 5.15.

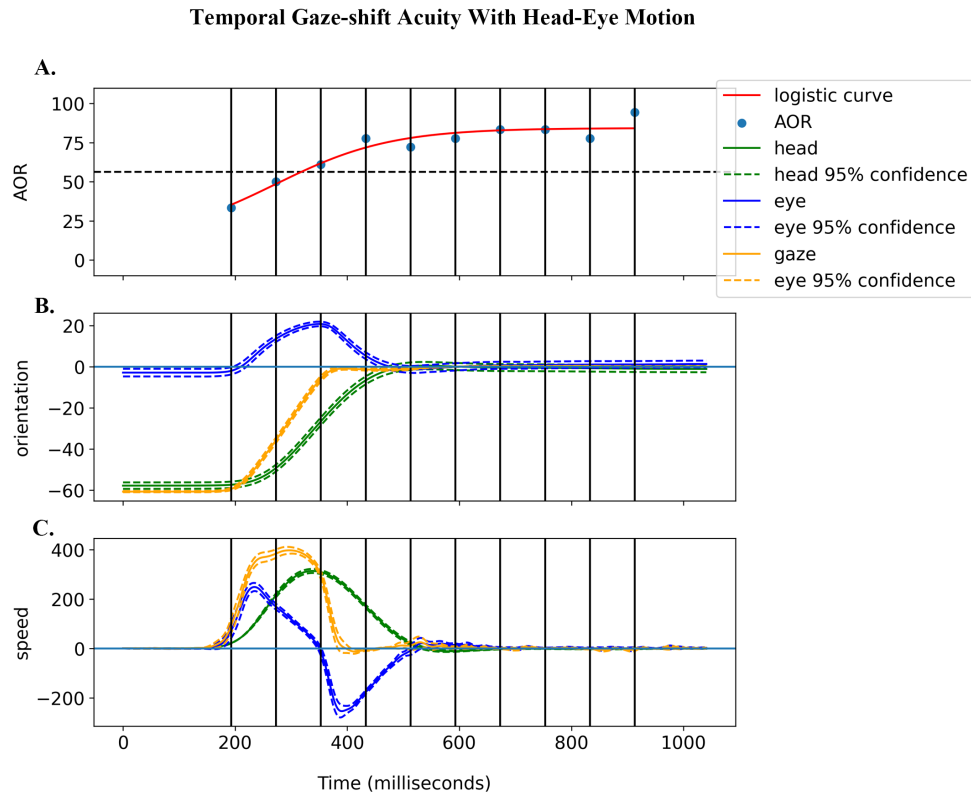


Figure 5.15: Combination data of gaze-shift task. Subplot A shows AOR of gaze-shift visual acuity. The y-axis represents the AOR. Subplot B shows orientation data of the head, eyes, and gaze. The y-axis represents the orientation in degrees. Subplot C shows angular velocity data of the head, eyes, and gaze. The y-axis represents the velocity in degrees per second. Shared x-axis: time of milliseconds.

Same as the TDVA analyses, we defined the time at which the head speed reached 5 degrees per second as the start of the head-turn. We see that at the beginning of the head-turn (from around 200 ms to 350 ms), the gaze speed is very high (maximum

at 390 degrees per second). Another fact is the eye hasn't reached the target yet so the optotype is out of fovea. Both of these reasons probably resulted in this subject resolved the optotype poorly. At the time stamp around 400 ms, which the gaze speed was nearly zero, the AOR increased to 77.8%, which surpassed the threshold. Thus the re-fixation time for the gaze-shift tasks for this subject is around 200 ms.

Chapter 6

Discussion

6.1 Key Findings

The key contribution of this work is an intervention and assessment framework for improving the precision of head and eye coordination for people who do not respond well to conventional vestibulo-ocular reflex dysfunction treatments. This includes the design and implementation of an innovative suite of virtual reality video games for training precise head rotation and a first-of-its-kind virtual environment display system that can assess visual acuity and gaze stability time delays simultaneously. Four head-rotation-controlled video games were designed to train fundamental neck movement control skills that span the continuum of from point-to-point motion (required by Ice Fisher and Meteor Defense) to high-velocity trajectory tracing (required by Slicer/Dicer), as well as functional integration of head and eye coordination (required by Blockbuster). The games were developed to maximize clinical viability by running on consumer-grade head-mounted virtual reality displays that are suitable for therapy clinics as well as home use. This is critical since conventional rehabilitation therapies for vestibular impairment can last months and includes both clinic and home exercises. Furthermore, the video games were refined with feedback from both vestibular

therapists and people with vestibular dysfunction. The developed intervention and assessment system is a necessary first step that enables additional studies to determine the clinical efficacy and therapeutic effect of treating people with vestibular dysfunction and do not respond to conventional VOR adaptation exercises.

Although conducting clinical trials of the video games were beyond the scope of this thesis, the current work did demonstrate the feasibility of using a unique virtual environment display to assess gaze stability timing delay in people with and without vestibular dysfunction. To the best of our knowledge, no one has developed a virtual environment to quantify the temporal aspects of gaze shifts related to head rotations, which are important for visual function. Additionally, using dual, calibrated high pixel density displays, the current work's virtual environment display system overcomes the visual acuity and head range of motion limitations of using one computer display. No single virtual reality or computer displays exist that can provide a field-of-view to match the range of motion of the head and visual acuity capability of the eye's fovea. A standard 24" 1080p computer monitor has the PPI of 91.7, which only provides LogMAR -0.32 (gap of one pixel) and 0.15 (gap of three pixels) optotypes when it is placed two meters away from the participants. This made the size between LogMAR -0.32 and 0.15 not testable. Moving the monitor farther away can increase visual resolution, but this limits the field of view. We designed a dual monitor system as a novel virtual environment interface to assess the gaze-shift movement. Therapists can now choose any position for these monitors, which made it possible that the test angle of the gaze-shift tasks can be potentially limitless. When placed at 1.5 meter away from the participant, the smallest (gap of one pixel) optotype that can be displayed by the developed system is equivalent to logMAR -0.88. and the second smallest (gap of three pixels) optotype is equivalent to logMAR -0.40. This system is potentially transformative for vestibular medicine because it can potentially provide clinicians and scientists insight into the effect that vestibular impairment has

on everyday visual function.

A key software contribution of the current project was a novel software architecture that integrated clinical sensors for measuring head and eye coordination. We used UDP networking to interface with head and eye motion sensor data from separate devices that were not originally designed to work with Unity 3D virtual environments, but are critical for assessing temporal dynamic acuity and temporal gaze-shift performance. Furthermore, we designed novel analysis scripts in Python to analyze the head-eye coordination data recorded from the Simulink system, as well as the acuity data. We are able to combine and synchronize the time stamps for the temporal AOR data with the head-eye orientation and head-eye angular velocity. These software tools are important for analyzing and diagnosing the re-fixation feature for both TDVA and TGVA tests, which were previously not studied, and will advance the vestibular science field.

Through the experiments from the TDVA tests (see section 4.2.4), we demonstrated that this software could accurately measure the visual patterns in HIT tasks and the TDVA. As shown in Figure 5.13, the AOR increased while the gaze velocity was close to zero. This shows that the AOR is negatively related to the gaze velocity, which is consistent with the theory that unsteady images projected on the retina will cause blurred vision (see section 2.2). This is important since the TDVA could contribute to clinically VOR diagnoses since it can reveal the re-fixation time from the HIT process, which has not been tested in normal VOR tests.

Another key finding is that we have discovered the characteristics of the TGVA and vision patterns during the gaze-shift tasks. As shown in Figure 5.14, among the gaze-shift process, healthy individuals turn their head and eyes almost simultaneously, but the head may lag behind due to the angular velocity differences between the head and eyes. This will result in the eyes reaching the target before the head. Then, using the VOR, the head catches up and rotates to match the eyes while the eyes are

fixated on the target. This is important since clinically, the VOR is mostly measured with a single focus spot such as in HIT and DVA tests, which are not similar vision patterns during activities of daily living. Gaze-shift testing and training may help people with vestibular impairment improve as they are closer to normal life activities (see Section 2.4).

Furthermore, as shown in Figure 5.15, TGVA tests can also reveal insights about the vision pattern during the gaze-shift process. Based on our results, the AOR would be very low at the beginning of the head-turn when the participants were not able to see the optotype without the head-turn. After the head-turn started, the AOR would rise as the eyes start to be able to fix on the target spot. The average re-fixation time from the healthy individuals was 290 ms. This means healthy individuals in this experiment may start to achieve visual stability at 290 ms after head-turn when the gaze-shift angle is 70 degrees.

6.2 Conclusion

We designed a VOR functional assessment interface that could assess the head-eye trajectories and vision re-fixation time during the TDVA and TGVA tests. We also utilized this interface and conducted experiments on six healthy individuals. We confirmed our hypothesis that the AOR negatively correlates with the gaze angular velocity during TGVA tasks. We also designed the Head Rotation Training Video Games with a commercial HMD VR headset, aiming for immersive training for VOR rehabilitation.

6.3 Limitation and Future Work

In these thesis experiments, we only used six healthy individuals as subjects due to time limitations. One of the subjects that remain to be explored is how the charac-

teristics of TDVA and TGVA are related to the severity of the VOR dysfunctions. Another limitation is during the DVA and TDVA tests, the subjects' vision may be interfered by the edge of the glasses lens if they were wearing one. Thus, the results of the DVA and TDVA tests were not precisely accurate for those individuals.

Future studies could conduct the TDVA and TGVA tests on people with VOR dysfunctions for more data. The effect of the Head Rotation Training Video Games should also be studied.

Bibliography

- [1] B. staff, “Medical gallery of blausen medical 2014,” *WikiJournal of Medicine* 1, 2014.
- [2] Aashmango4793. (2019) Svg orthographic projection denoting roll, yaw and pitch axes in an aircraft. [Online]. Available: https://commons.wikimedia.org/wiki/File:Flight_dynamics_with_text_ortho.svg
- [3] E. Britannica. vestibular system. [Online]. Available: <https://www.britannica.com/science/cupula/images-videos#/media/1/146763/68878>
- [4] D. Alyahya, E. Johnson, N. Daher, S. Gaikwad, S. Deshpande, T. Cordett, and L. Zidek, “Effect of vestibular adaptation exercises on chronic motion sensitivity: a randomized controlled trial,” *Physical Therapy and Rehabilitation*, vol. 3, p. 1, 01 2016.
- [5] J. Feasel, M. C. Whitton, L. Kassler, F. P. Brooks, and M. D. Lewek, “The integrated virtual environment rehabilitation treadmill system,” *IEEE Transactions on Neural Systems and Rehabilitation Engineering*, vol. 19, no. 3, pp. 290–297, 2011.
- [6] R. J. Leigh and D. S. Zee, *The neurology of eye movements*. OUP USA, 2015.
- [7] F. Miles and S. Lisberger, “Plasticity in the vestibulo-ocular reflex: a new hypothesis,” *Annual review of neuroscience*, vol. 4, no. 1, pp. 273–299, 1981.
- [8] H. N. A. I. Yasuo Harada, Masaki Taniguchi, “Magnetic materials in otoliths of bird and fish lagena and their function,” *Acta Oto-Laryngologica*, vol. 121, no. 5, pp. 590–595, 2001. [Online]. Available: <https://doi.org/10.1080/00016480118968>
- [9] D. E. Angelaki and K. E. Cullen, “Vestibular system: The many facets of a multimodal sense,” *Annual Review of Neuroscience*, vol. 31, no. 1, pp. 125–150, 2008, pMID: 18338968. [Online]. Available: <https://doi.org/10.1146/annurev.neuro.31.060407.125555>
- [10] G. M. Jones and J. Milsum, “Characteristics of neural transmission from the semicircular canal to the vestibular nuclei of cats,” *The Journal of physiology*, vol. 209, no. 2, pp. 295–316, 1970.

- [11] ——, “Frequency—response analysis of central vestibular unit activity resulting from rotational stimulation of the semicircular canals,” *The Journal of physiology*, vol. 219, no. 1, pp. 191–215, 1971.
- [12] G. Melvill Jones, H. B. Barlow, and R. M. Gaze, “Plasticity in the adult vestibulo-ocular reflex arc,” *Philosophical Transactions of the Royal Society of London. B, Biological Sciences*, vol. 278, no. 961, pp. 319–334, 1977.
- [13] Y. Agrawal, B. K. Ward, and L. B. Minor, “Vestibular dysfunction: prevalence, impact and need for targeted treatment,” *Journal of vestibular research: equilibrium & orientation*, vol. 23, no. 3, p. 113, 2013.
- [14] M. von Brevern, “Benign paroxysmal positional vertigo,” in *Seminars in neurology*, vol. 33, no. 03. Thieme Medical Publishers, 2013, pp. 204–211.
- [15] H. K. Neuhauser, A. Radtke, M. Von Brevern, F. Lezius, M. Feldmann, and T. Lempert, “Burden of dizziness and vertigo in the community,” *Archives of internal medicine*, vol. 168, no. 19, pp. 2118–2124, 2008.
- [16] Y. Agrawal, J. P. Carey, C. C. Della Santina, M. C. Schubert, and L. B. Minor, “Disorders of Balance and Vestibular Function in US Adults: Data From the National Health and Nutrition Examination Survey, 2001-2004,” *Archives of Internal Medicine*, vol. 169, no. 10, pp. 938–944, 05 2009. [Online]. Available: <https://doi.org/10.1001/archinternmed.2009.66>
- [17] B. K. Ward, Y. Agrawal, H. J. Hoffman, J. P. Carey, and C. C. Della Santina, “Prevalence and impact of bilateral vestibular hypofunction: results from the 2008 us national health interview survey,” *JAMA otolaryngology-head & neck surgery*, vol. 139, no. 8, pp. 803–810, 2013.
- [18] M. B. Liston, D.-E. Bamiou, F. Martin, A. Hopper, N. Koohi, L. Luxon, and M. Pavlou, “Peripheral vestibular dysfunction is prevalent in older adults experiencing multiple non-syncopal falls versus age-matched non-fallers: a pilot study,” *Age and ageing*, vol. 43, no. 1, pp. 38–43, 2014.
- [19] S. J. Herdman, P. Blatt, M. C. Schubert, and R. J. Tusa, “Falls in patients with vestibular deficits,” *Otology & Neurotology*, vol. 21, no. 6, pp. 847–851, 2000.
- [20] C. D. Hall, S. J. Herdman, S. L. Whitney, S. P. Cass, R. A. Clendaniel, T. D. Fife, J. M. Furman, T. S. Getchius, J. A. Goebel, N. T. Shepard *et al.*, “Vestibular rehabilitation for peripheral vestibular hypofunction: an evidence-based clinical practice guideline: from the american physical therapy association neurology section,” *Journal of Neurologic Physical Therapy*, vol. 40, no. 2, p. 124, 2016.
- [21] E. E. Hansson and M. Magnusson, “Vestibular asymmetry predicts falls among elderly patients with multi-sensory dizziness,” *BMC geriatrics*, vol. 13, no. 1, p. 77, 2013.

- [22] J. A. Stevens, P. S. Corso, E. A. Finkelstein, and T. R. Miller, "The costs of fatal and non-fatal falls among older adults," *Injury prevention*, vol. 12, no. 5, pp. 290–295, 2006.
- [23] R. M. Yoder and J. S. Taube, "The vestibular contribution to the head direction signal and navigation," *Frontiers in integrative neuroscience*, vol. 8, p. 32, 2014.
- [24] R. T. Bigelow, Y. R. Semenov, C. Trevino, L. Ferrucci, S. M. Resnick, E. M. Simonsick, Q.-L. Xue, and Y. Agrawal, "Association between visuospatial ability and vestibular function in the baltimore longitudinal study of aging," *Journal of the American Geriatrics Society*, vol. 63, no. 9, pp. 1837–1844, 2015.
- [25] V. C. Zingler, C. Cnyrim, K. Jahn, E. Weintz, J. Fernbacher, C. Frenzel, T. Brandt, and M. Strupp, "Causative factors and epidemiology of bilateral vestibulopathy in 255 patients," *Annals of Neurology*, vol. 61, no. 6, pp. 524–532, 2007. [Online]. Available: <https://onlinelibrary.wiley.com/doi/abs/10.1002/ana.21105>
- [26] B. K. Ward, A. Wenzel, R. R. Kalyani, Y. Agrawal, A. L. Feng, M. Polydefkis, H. S. Ying, M. C. Schubert, M. G. Zuniga, C. C. D. Santina, and J. P. Carey, "Characterization of vestibulopathy in individuals with type 2 diabetes mellitus," *Otolaryngology—Head and Neck Surgery*, vol. 153, no. 1, pp. 112–118, 2015, PMID: 25829391. [Online]. Available: <https://doi.org/10.1177/0194599815576717>
- [27] M. Scherer, H. Burrows, R. Pinto, and E. Somrak, "Characterizing Self-Reported Dizziness and Otovestibular Impairment among Blast-Injured Traumatic Amputees: A Pilot Study," *Military Medicine*, vol. 172, no. 7, pp. 731–737, 07 2007. [Online]. Available: <https://doi.org/10.7205/MILMED.172.7.731>
- [28] C. Li, A. J. Layman, R. Geary, E. Anson, J. P. Carey, L. Ferrucci, and Y. Agrawal, "Epidemiology of vestibulo-ocular reflex function: data from the baltimore longitudinal study of aging," *Otology & neurotology: official publication of the American Otological Society, American Neurotology Society [and] European Academy of Otology and Neurotology*, vol. 36, no. 2, p. 267, 2015.
- [29] R. Baloh, K. Jacobson, and T. Socotch, "The effect of aging on visual-vestibuloocular responses," *Experimental brain research*, vol. 95, no. 3, pp. 509–516, 1993.
- [30] K. Brantberg, K. Granath, and N. Schart, "Age-related changes in vestibular evoked myogenic potentials," *Audiology and Neurotology*, vol. 12, no. 4, pp. 247–253, 2007.
- [31] I. Lopez, G. Ishiyama, Y. Tang, J. Tokita, R. W. Baloh, and A. Ishiyama, "Regional estimates of hair cells and supporting cells in the human crista ampullaris," *Journal of neuroscience research*, vol. 82, no. 3, pp. 421–431, 2005.

- [32] U. Rosenhall and W. Rubin, “Degenerative changes in the human vestibular sensory epithelia,” *Acta oto-laryngologica*, vol. 79, no. 1-2, pp. 67–80, 1975.
- [33] M. Gleeson and H. Felix, “A comparative study of the effect of age on the human cochlear and vestibular neuroepithelia,” *Acta Oto-laryngologica*, vol. 104, no. sup436, pp. 103–109, 1987.
- [34] R. R. Taylor, D. J. Jagger, S. R. Saeed, P. Axon, N. Donnelly, J. Tysome, D. Moffatt, R. Irving, P. Monksfield, C. Coulson *et al.*, “Characterizing human vestibular sensory epithelia for experimental studies: new hair bundles on old tissue and implications for therapeutic interventions in ageing,” *Neurobiology of aging*, vol. 36, no. 6, pp. 2068–2084, 2015.
- [35] J. J. Park, Y. Tang, I. Lopez, and A. Ishiyama, “Age-related change in the number of neurons in the human vestibular ganglion,” *Journal of Comparative Neurology*, vol. 431, no. 4, pp. 437–443, 2001.
- [36] I. Lopez, V. Honrubia, and R. W. Baloh, “Aging and the human vestibular nucleus,” *Journal of Vestibular Research*, vol. 7, no. 1, pp. 77–85, 1997.
- [37] U. Rosenhall, “Degenerative patterns in the aging human vestibular neuroepithelia,” *Acta oto-laryngologica*, vol. 76, no. 1-6, pp. 208–220, 1973.
- [38] L. Walther and M. Westhofen, “Presbyvertigo-aging of otoconia and vestibular sensory cells,” *Journal of Vestibular Research*, vol. 17, no. 2, 3, pp. 89–92, 2007.
- [39] K. Weber, S. Aw, M. Todd, L. McGarvie, I. Curthoys, and G. Halmagyi, “Head impulse test in unilateral vestibular loss: vestibulo-ocular reflex and catch-up saccades,” *Neurology*, vol. 70, no. 6, pp. 454–463, 2008.
- [40] B. Mossman, S. Mossman, G. Purdie, and E. Schneider, “Age dependent normal horizontal vor gain of head impulse test as measured with video-oculography,” *Journal of Otolaryngology-Head & Neck Surgery*, vol. 44, no. 1, p. 29, 2015.
- [41] H. MacDougall, K. Weber, L. McGarvie, G. Halmagyi, and I. Curthoys, “The video head impulse test: diagnostic accuracy in peripheral vestibulopathy,” *Neurology*, vol. 73, no. 14, pp. 1134–1141, 2009.
- [42] L. N. Reich and M. Ekabutr, “The effects of optical defocus on the legibility of the tumbling-e and landolt-c,” *Optometry and Vision Science*, vol. 79, no. 6, pp. 389–393, 2002.
- [43] A. T. Chau, J. C. Menant, P. P. Hübner, S. R. Lord, and A. A. Migliaccio, “Prevalence of vestibular disorder in older people who experience dizziness,” *Frontiers in neurology*, vol. 6, p. 268, 2015.
- [44] M. C. Schubert, A. A. Migliaccio, R. A. Clendaniel, A. Allak, and J. P. Carey, “Mechanism of dynamic visual acuity recovery with vestibular rehabilitation,” *Archives of physical medicine and rehabilitation*, vol. 89, no. 3, pp. 500–507, 2008.

- [45] D. Vital, S. C. Hegemann, D. Straumann, O. Bergamin, C. J. Bockisch, D. Angehrn, K.-U. Schmitt, and R. Probst, “A new dynamic visual acuity test to assess peripheral vestibular function,” *Archives of Otolaryngology–Head & Neck Surgery*, vol. 136, no. 7, pp. 686–691, 2010.
- [46] J. A. Honaker and N. T. Shepard, “Use of the dynamic visual acuity test as a screener for community-dwelling older adults who fall,” *Journal of Vestibular Research*, vol. 21, no. 5, pp. 267–276, 2011.
- [47] J. T. Holladay, “Proper method for calculating average visual acuity,” *Journal of refractive surgery*, vol. 13, no. 4, pp. 388–391, 1997.
- [48] J. S. Stahl, “Amplitude of human head movements associated with horizontal saccades,” *Experimental brain research*, vol. 126, no. 1, pp. 41–54, 1999.
- [49] R. Black, G. Halmagyi, I. S. Curthoys, M. Thurtell, and A. Brizuela, “Unilateral vestibular deafferentation produces no long-term effects,” *Experimental brain research*, vol. 122, no. 3, pp. 362–366, 1998.
- [50] T. Kasai and D. Zee, “Eye-head coordination in labyrinthine-defective human beings,” *Brain research*, vol. 144, no. 1, p. 123—141, April 1978. [Online]. Available: [https://doi.org/10.1016/0006-8993\(78\)90439-0](https://doi.org/10.1016/0006-8993(78)90439-0)
- [51] M. Dix and C. Hallpike, “The pathology, symptomatology and diagnosis of certain common disorders of the vestibular system,” 1952.
- [52] M. Pavlou, R. Kanegaonkar, D. Swapp, D. Bamiou, M. Slater, and L. Luxon, “The effect of virtual reality on visual vertigo symptoms in patients with peripheral vestibular dysfunction: a pilot study,” *Journal of vestibular research*, vol. 22, no. 5, 6, pp. 273–281, 2012.
- [53] H. S. Cohen, H. Sangi-Haghpeykar, N. A. Ricci, J. Kampangkaew, and R. A. Williamson, “Utility of stepping, walking, and head impulses for screening patients for vestibular impairments,” *Otolaryngology–Head and Neck Surgery*, vol. 151, no. 1, pp. 131–136, 2014.
- [54] N. H. Hughes, “Quaternion to euler angle conversion for arbitrary rotation sequence using geometric methods,” Accessed online at noelhughes.net/uploads/quat, vol. 2, 2008.
- [55] M. Bach *et al.*, “The freiburg visual acuity test-automatic measurement of visual acuity,” *Optometry and vision science*, vol. 73, no. 1, pp. 49–53, 1996.